Two examples of ratchet processes in microfluidics

Hanyang Wang

Thesis submitted to the
Faculty of Graduate and Postdoctoral Studies
In partial fulfillment of the requirements
For the Master's degree in Physics

Ottawa-Carleton Institute of Physics
Department of Physics
Faculty of Science
University of Ottawa

Summary

The ratchet effect can be exploited in many types of research, yet few researchers pay attention to it. In this thesis, I investigate two examples of such effects in microfluidic devices, under the guidance of computational simulations.

The first chapter provides a brief introduction to ratchet effects, electrophoresis, and swimming cells, topics directly related to the following chapters. The second chapter of this thesis studies the separation of charged spherical particles in various microfluidic devices. My work shows how to manipulate those particles with modified temporal asymmetric electric potentials.

The rectification of randomly swimming bacteria in microfluidic devices has been extensively studied. However, there have been few attempts to optimize such rectification devices. Mapping such motion onto a lattice Monte Carlo model may suggest some new mathematical methods, which might be useful for optimizing the similar systems. Such a mapping process is introduced in chapter four.

Sommaire

L'effet de cliquet (plus connu sous le nom anglais de ⟨ratchet⟩) peut être exploité dans le cadre de nombreux types de problèmes scientifiques. Cependant, peu de chercheurs s'y intéressent. Dans cette thèse, j'explore deux exemples de ce phénomène dans des systèmes microfluidiques à l'aide de simulations numériques.

Le premier chapitre présente une brève introduction des effets de type ratchet, de l'électrophorèse et de la motilité cellulaire. Le second chapitre étudie la séparation de particules sphériques chargées dans différents systèmes microfluidiques. Mon travail montre comment manipuler ces particules dans des potentiels électriques temporellement asymétriques.

La rectification de la marche aléatoire des bactéries dans les systèmes microfluidiques a été passablement étudiée. Cependant il y a eu peu de tentatives d'optimisation de ces systèmes. La représentation d'un tel processus de ratchet par un modèle simple de type Monte Carlo pourrait mener à la mise au point de nouvelles méthodes mathématiques utiles pour optimiser la performance de ces dispositifs. Une telle représentation est introduite au chapitre quatre.

Statement of Originality

The research presented in the following thesis came out of my training as a Master candidate. Unless otherwise noted, I have produced all of the plots and schematics.

The work presented in the second chapter is ready to be submitted. Previous group members Antoine Dube and Hendrick de Haan have done some of the preliminary work on this topic. However, all of the simulation data, the theoretical derivations, and the analysis presented in Chapter 2 are my original work.

Previous group members Y. Tao, Hendrick de Haan and M. Bertrand have done some of the preliminary work related to the concepts in Chapter 4. I declare that all of the simulation data and the analysis in Chapter 4 are my original work. The manuscript of the fourth chapter of this thesis will be finished shortly and submitted for publication.

The simulations in this thesis were mostly based on different versions of the simulation package ESPResSo which was modified by myself. The data analysis was carried out using routines coded in Python.

Acknowledgements

I have been fortunate to have Gary Slater as my supervisor. Thank you for introducing me to this field. Thank you for offering guidance in my research. Thank you for feeding my curiosity. Your enthusiasm and knowledge have always been a great source of inspiration. I appreciate the huge amount of time you spent helping me during these years.

Gary's research group has played an important role in my working environment. I would give thanks to all my colleagues. I would like to thank David for his patient help with the simulations. Le for his wise suggestions. Max for distracting me from time to time and teaching me how to become a qualified researcher. Mykyta for sharing his wealth of knowledge. Mehran for being an endless source of discussion. Neo for teaching me some French, Sab for the random visits and entertaining conversations.

I would also like to thank Hendrick for his word of wisdom, for his generous help on my first project. I would like to thank Y. Tao and M. Bertrand for their preliminary but very important work on the rectification of swimming cells.

I am forever grateful to my parents, Liqun and Yongmin, who provided me with the foundation and supported me with patience and love.

For my grandmother

Contents

Chapter 1

Introduction

My thesis contains two major parts: one relates to the theory of charged particles separation using electrophoretic techniques, while the other investigates mapping the dynamics of active cells onto a lattice Monte Carlo model. Both of them explore ratchet effects.

In order to build theoretical models, both projects are based on computational simulation methods. Computational simulations have become more important with the development of powerful hardware and technology. Simulation approaches have grown fast and steadily. New ideas and assumptions can be tested easily using such approaches.

The ratchet effect we consider is different from the idea readers may have. When the word "ratchet" is mentioned, the first things that come mind might be gears or screws. However the meaning of "ratchet" has expanded over the last century; for instance, it can also refer to directional transport in scientific research. The ratchet effect is an interesting and potentially powerful method for purifying, separating and moving target particles or molecules, yet few researchers

pay attention to it. Many possible applications have not been discussed or even tested till now. As examples of possible applications, in the first project, we use the ratchet effect to manipulate charged particles by electrophoresis, while in the second project we explore the rectification of the stochastic-self-driven active matter inside a system of funnels.

Electrophoresis is considered as the most versatile separation method in biology and macromolecular research [1–3]. However, it is sometimes a rather weak separation technique. For example, in the case of long charged polymers (e.g. DNA chains) in free solution, the longer the DNA chains are, the weaker the separation will be. The local balance between the electric force and the friction determines the DNA chain's velocity in free solution. Due to the nature of electro-hydrodynamics, for long DNA chains, the electric force is proportional to the number of bases N (the charge q is proportional to N), but the friction coefficient ξ also grows linearly as the number of bases increases [4]. The velocity is length-independent: $v \sim qE/\xi \sim N^1/N^1 \sim N^0$. Without a length-dependent velocity, the separation of DNA using electrophoresis in free solution obviously fails.

Although using free solution electrophoresis as a separation technique is less reliable for DNA, introducing other components into the system, like microfluidic sieving devices, gels and so on, may allow long DNA chains to be separated. Similar situations may occur when separating particles, for example, particles might have the same net velocity in free-flow electrophoresis; the challenge is then to separate those particles by introducing other components into a microfluidic device. Such devices may contain alternating wells and

slits to separate particles that cannot be separated by free flow electrophoresis. Additionally, introducing a ratchet effect into such a system, thus forcing particles to move towards different directions, is also possible. One of the main subjects of this thesis is related to this topic.

Rectifying the motion of active matter, more specifically Escherichia coli (E. coli) in our case, has become a hot research area. E. coli lives in our guts and has a symbiotic relationship with us. It is one of the simplest and oldest living creatures on Earth. As a living cell, E. coli can move and multiply; with enough food and a suitable environment, E. coli can continue those activities for a long time [5]. The motion of E. coli has been extensively studied, and the theory agrees with experimental results. Studying the rectification of the motion of active cells is also important in many parts of biology.

How can we concentrate or separate such moving active matter? Common approaches include the funnel structure device, the membraneless H filter, the microfluidic T sensor [6], etc. All of these devices are powerful tools. However, there are few models to optimize them. Mapping such motion onto a lattice Monte Carlo model may suggest some new mathematical methods, which can be used to optimize the rectification effects of similar devices.

This chapter provides a brief introduction to the ratchet effect, the electrophoresis of particles, active matter and simulation methods.

In this thesis, I will be focusing on how to separate charged spherical particles in some microfluidic devices (Chapter 2), and how to using temporal asymmetric electric potential to manipulate those particles at will (Chapter 2 and 3). I also propose a simple empirical stretched

exponential function to describe the field-dependence of the particles' mobility (Chapter 2).

In Chapter 4, I investigate the possibility of mapping the dynamics of swimming cells onto a simple one dimensional lattice biased random walk model.

In the conclusion, I discuss different applications and extensions of the work presented in the thesis. Many more questions are waiting to be answered.

1.1 Ratchets

Traditionally, a ratchet is a process that is forcing one object to move linearly in one direction in the system, while preventing the motion in the opposite direction. Common examples include mechanical designs of gears and screws. However, in biophysics research and applications, the ratchet is also as a mechanism for directional transport. It was discussed by Smoluchowski in 1912 [7]. Feynman's research about two thermal heat baths with different temperatures can be considered as a simple form of ratchet system as well [8]. In biochemistry and biophysics, the ratchet effect is central to the physics of molecular motors and molecular pumps [9], as many experiments have shown since the mid-1970s. However, the ratchet effect is still a new concept in many fields of research. The advantages of using the ratchet process have probably been underestimated by many researchers.

In order to obtain the ratchet effect, two basic conditions are required for every system: non-equilibrium and an asymmetry. To

add a non-equilibrium component, an external source of perturbation (deterministic or stochastic) is required [9], such as a zero-mean alternating field or non-Brownian random motion. The breaking of the inversion symmetry is also an indispensable condition for directional transport. How can we satisfy these conditions? The methods for achieving these two requirements are both simple and diverse.

The non-equilibrium component can come from an external force, entropic potentials in the system, or a combination of these two. For instance, in a thermal ratchet (e.g., a Brownian motor), the system will be driven away from thermal equilibrium by an additional perturbation, a common approach being a second thermal heat bath in the system [9]. In some and probably the most interesting ratchet systems, the perturbation is unbiased, that is, time- or space-averaged forces are required to vanish, yet the net motion of the target object is not zero inside asymmetric systems.

The ratchet symmetry-breaking requirement can be achieved using asymmetric substrates, asymmetric driving or a combination of the two. The spatial asymmetry is simply provided by the geometric design of the system. Irregularly shaped barriers, entries with different widths, specially designed chambers, and funnel structures are common instances. The temporal asymmetry, on the other hand, can be implemented by using alternative fields with unequal durations or amplitudes.

A ratchet system based on temporal asymmetry also requires a velocity which changes nonlinearly as the magnitude of the perturbation changes. Using alternating fields as an example, switching the direction with unequal pulse durations and amplitudes, the net

displacements in these two directions are not equal due to the non-linear velocity with respect to the field intensity. Ratchets based on both temporal asymmetries and spatial symmetry-breaking geometries have played important roles in my projects.

Using the ratchet effect, one can manipulate the system at will. Common applications include: selecting specific objects from a mixture, accumulating or separating objects, etc. The most interesting ratchet result would be absolute negative mobility (ANM). ANM is a phenomenon characterized by the fact that the response of the system is in a different direction than the net driving force. My first project investigates the manipulation of charged particles and shows how to obtain ANM.

Of course, temporal ratchet effects are useful in many applications, but most ratchet systems use spatial asymmetry. In the second project of this thesis, we use a simple funnel-shape system to study the rectified motion of active matter. Those active matter elements can accumulate towards the direction that the funnels point to. The special geometry helps the mobile agents move in one direction while restricting their motion in the opposite direction.

1.2 Electrophoresis

1.2.1 Basic Principle

Electrophoresis was invented in 1807 by Russian researchers Strakhov and Reuss [10] . Their experiments investigated the motion of charged clay particles in an aqueous solution, under the effect of an electric field. They discovered that clay particles formed patterns. Those

patterns meant that charged clay particles were driven at different velocities under the same electric field. Many techniques of separating charged objects were invented since then.

Electrophoresis is a powerful method for separating charged objects, including polymers, colloids, and many more molecules in general. However, in some cases, it fails as a separation technique. As mentioned in the previous section, the electrophoretic velocity of any long, flexible and uniformly charged DNA is length-independent. Researchers have observed that DNA velocities lose their size dependence when the number of bases increases beyond 400-500 bp for dsDNA [11]. However for short DNA fragments, up to 20 bases for ssDNA and 170 bp for dsDNA [11], because of chain end effects, good separation can be achieved. To separate long DNA molecules, gel electrophoresis was introduced in the 1930s [12]. The principles of gel electrophoresis are straight-forward: the network of gel fibers allows small DNA molecules to travel faster than large molecules. In a gel, longer DNA collide more frequently with fibers, thus the separation by length can be expected [12].

Due to the nature of DNA, long DNA chains can not be separated in free solution. However, the situation is different for charged particles. Many factors affect the velocity of charged particles in an electric field, including hydrodynamics, the concentration of particles, the charge distribution on the surface of the particles, the properties of the solvents and so on. In some cases, those factors may make some nano- or micro-particles fail to separate in free flow electrophoresis. In order to achieve good separation, a different approach is then required, just like introducing gel in DNA electrophoresis. This will be addressed later in this Chapter.

In general, electrophoresis of charged objects in an ion-rich aqueous environment is a competition between electrical, viscous and retardation forces. Counter-ions with the opposite charge form a "layer" around charged objects in solution. The thickness of this layer, the so-called Debye length λ_D, is the key parameter to distinguishing the various situations. The electric field pulls the charged object in one direction. The counter-ions around the objects also feel a force in the opposite direction and drag the fluid with them when they move. The charged object will feel the drag force not only due to the fluid but also due to the moving counter-ions and the related electroosmotic flow. The drag force due to the counter-ions flow is called the retardation force. At the same time, the ionic atmosphere lags slightly behind charged objects, which results in a small electric force in the opposite direction: this is the term called relaxation effect [13]. The total force applied to a particle during electrophoresis is thus given by:

$$\vec{F}_{total} = \vec{F}_E + \vec{F}_f + \vec{F}_{ret} + \vec{F}_{rel} + \vec{F}_B = 0. \tag{1.1}$$

In Eq. (1.1), $\vec{F}_E$ is the electrical force, $\vec{F}_f$ is the drag force, $\vec{F}_{ret}$ is the retardation force, $\vec{F}_{rel}$ is caused by the relaxation effect, and $\vec{F}_B$ is the Brownian force.

In a solvent, the relaxation time of a Brownian particle is generally in the range from 10^{-8} to 10^{-6} second. For instance, at room temperature, a silica microsphere particle with a 1 μm diameter has a relaxation time of 1.1×10^{-7} second [14]. For times shorter than the relaxation time a Brownian particle follows "ballistic Brownian motion". Over this timescale detailed interactions between the Brownian particle and the solvent molecules cannot be ignored. However,

such times are typically much smaller than the timescale over which the conservative forces change; in this overdamped limit we may set the acceleration of the particle to zero, thus the total force $\vec{F}_{total}$ is zero.

However, the forces in Eq. (1.1) are strongly case dependent. Most of the time, the relaxation effect $\vec{F}_{rel}$ can be neglected [13]. The electrical force $\vec{F}_E$ depends on the charge of the object and the field strength, the drag force due to the fluid $\vec{F}_f$ depends on the shape of the object, and the retardation force $\vec{F}_{ret}$ depends on the thickness of the counter-ions layer (λ_D) and the surface potential ζ. The local balance between these forces determines the velocity of a charged particle. In the following subsection, we will discuss different limit cases for a uniformly charged spherical particle.

1.2.2 Electrophoresis of Charged particles

For a spherical particle with a charge q in the presence of an electric field $\vec{E}$, the electrical force acting on it is simply

$$\vec{F}_E = q\vec{E}. \tag{1.2}$$

In a liquid, the dissipative drag force pulls the particle in the opposite direction. This force is expressed as

$$\vec{F}_f = -\xi\vec{v}, \tag{1.3}$$

where $\vec{v}$ is the velocity of the particle and the parameter ξ is the friction coefficient. A spherical particle has a friction coefficient

$$\xi = 6\pi\eta R, \tag{1.4}$$

where η is the viscosity of the liquid describing the internal resistance of the medium during the flow, and R is the radius of the particle.

1.2.2.1 Case one: small particles

As mentioned before, the retardation forces are case dependent. When the Debye length is much larger than the size of the particle ($\lambda_D \gg R$), the retardation force is too weak to be noticed. In this situation, when the steady state is reached, the forces are balanced:

$$\vec{F}_f = -\vec{F}_E. \tag{1.5}$$

Putting Eqs. (1.1) - (1.5) together, the expression for a particle net electrophoretic velocity in the solution is:

$$\vec{v} = \frac{\vec{F}_E}{\xi} = \frac{q\vec{E}}{6\pi\eta R}. \tag{1.6}$$

The net velocity depends on the ratio between the charge q and the particle radius R. In electrophoresis studies, one parameter called the mobility μ is often used. The electrophoretic mobility essentially describes the resistance to motion:

$$\mu \equiv \frac{|v|}{|E|} = \frac{q}{6\pi\eta R}. \tag{1.7}$$

It is important to stress the fact that Eq. (1.7) is only true when the Debye length is much larger than the size of the particle, as

Fig. 1.1(a) shows. For a small particle, such as an ion, the counter-ions transfer a very small amount of energy and momentum to the particle. The influence of the counter-ions is so small that we can neglect the retardation forces acting on the particle. As long as the ratio q/R differs between the particles, the latter can be separated by free-flow electrophoresis.

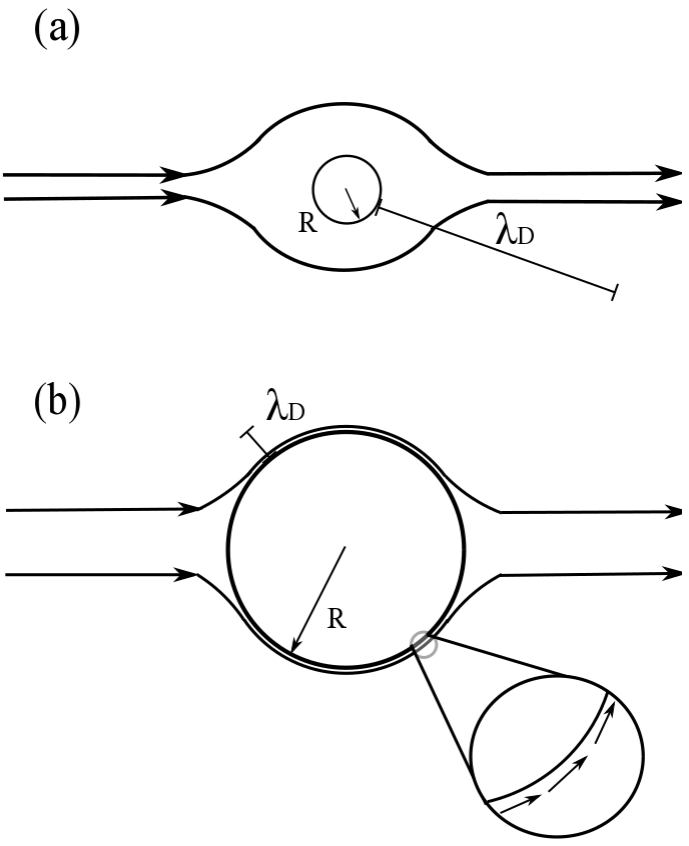

FIGURE 1.1: (a) Fluid flow around a spherical particle, when $R \ll \lambda_D$, and (b) when $R \gg \lambda_D$; R is the radius of the particle and λ_D is the Debye length of the solution.

1.2.2.2 Case two: large particles

However, when the Debye length is much smaller than the particle size ($\lambda_D \ll R$), the relationship above is not valid anymore (Fig.

1.1(b)). The friction between the particle and the counter-ions is then local: the transfer of energy and momentum between the particle and the fluid happens on a length scale λ_D. On this scale, the surface of the charged particle can be considered as flat: the hydrodynamic and electric field lines are thus essentially parallel. According to Smoluchowski [15], the expression for the electrophoretic velocity $\vec{v}$ is then simply

$$\vec{v} = \frac{\zeta \epsilon_r \epsilon_0}{\eta} \vec{E}, \tag{1.8}$$

where ϵ_r is the dielectric constant of the solution and ϵ_0 is the permittivity of free space. The mobility is thus given by

$$\mu = \frac{\zeta \epsilon_r \epsilon_0}{\eta}. \tag{1.9}$$

Equation (1.9) is the well known discovery made by Smoluchowski in 1903 [15]; it is called the Helmholtz-Smoluchowski equation for electrophoresis. The surface potential ζ depends on the charge and radius of the particle and on the Debye length of the solution [13]:

$$\zeta = \frac{\psi R}{\epsilon_r \epsilon_0 (1 + R/\lambda_D)}. \tag{1.10}$$

Here the parameter ψ is the net electrokinetic charge density and it describes the amount of charges on the particle ($\sim q/R^2$). Henry provided a solution for which is valid for all values of the ratio R/λ_D, and which takes into account the deformation of the electric field lines near the particles[17]:

$$\mu = \frac{2\epsilon_0 \epsilon_r \zeta}{3\eta} \, f\left(\frac{R}{\lambda_D}\right). \tag{1.11}$$

When $R/\lambda_D \ll 1$, the function $f(\frac{R}{\lambda_D}) = 1$ and the Henry equation reduces to Huckel's equation [16]:

$$\mu = \frac{2\epsilon_0\epsilon_r\zeta}{3\eta}. \tag{1.12}$$

In the limit where the size of the particle is small ($R \ll \lambda_D$), the ratio R/λ_D in the denominator in Eq. (1.10) is negligible and the surface potential is then $\zeta \sim qR/(4\pi R^2)$. Combining this relation with Eq. (1.9), we predict that the particle mobility then depends simply on the ratio q/R, which is exactly Eq. (1.7) under the same condition. In the limit where $R \gg \lambda_D$, the function $f(\frac{R}{\lambda_D}) = 3/2$, thus Eq. (1.11) reduces to Smoluchowski's solution (1.9). Since we obtain $\zeta \cong \frac{\psi\lambda_D}{\epsilon_r}$ in that limit, Eq. (1.9) then shows that the particle mobility has lost its size-dependence; it depends solely on the charge density ψ.

1.2.3 Simulating particle dynamics in a fluid

In order to investigate a simple situation where free flow electrophoresis fails completely, it is first necessary to state the theory and assumptions behind our simulation model.

Our spherical particle is placed in a solvent that can be treated as a heat bath. Collisions between solvent molecules and the particle impose random forces, which can cause directed motion or slow down an existing one. As a result of countless collisions, the particle will undergo Brownian motion. The random motion of that particle is what leads to diffusion. The diffusion coefficient D of a Brownian particle can be defined by how the particles' mean-squared displacement $\langle \Delta r^2 \rangle$ changes with time

$$\langle \Delta r^2 \rangle = 2dDt, \tag{1.13}$$

where d is the dimensionality of space. For a particle in solution, Brownian motion can be treated as the source of viscous and random forces.

The viscous force is described in Eqs. (1.3) and (1.4): the flow of solvent imposes a damping force that pulls moving particle in the opposite direction. Additionally, the solvent molecules randomly hit the particle to impose random forces. The solvent that provides such random forces has an energy scale $\sim k_B T$, where k_B is Boltzmann's constant, and T is the temperature of the solvent. The two viewpoints suggest that ξ and D must be related.

This is an example of a fluctuation-dissipation theorem. The solvent provides both the friction force and the diffusion force, as described by the coefficients ξ and D. The relationship between D and ξ is determined beautifully by the Einstein-Smoluchowski relation:

$$D = \frac{k_B T}{\xi}. \tag{1.14}$$

It is also important to mention that we are interested in the dynamics of the spherical Brownian particles in the presence of an external force. The simulation of these particles is based on the Langevin equation of motion [18]

$$m\ddot{\vec{r}} = \vec{F}_C - \xi(R)\dot{\vec{r}} + \vec{F}_B, \tag{1.15}$$

where $\vec{r}$ is the position of the particle having mass m, $\vec{F}_C$ is the sum of the conservative forces, $\xi(R)$ is the particle friction coefficient (as Eq. (1.4) shows, it is a function of its radius R for a spherical particle),

and $\vec{F}_B$ is the random Brownian force. As discussed previously, the role of the solvent is implicitly present in the last two terms in Eq. (1.15): $-\xi(R)\dot{\vec{r}}$ represents the viscous force and $\vec{F}_B$ accounts for the random collisions which cause Brownian motion. To simulate the random fluctuating forces, we use an uncorrelated random force $\vec{F}_B$ with the following properties for each dimension of space:

$$\begin{cases} \langle F_B \rangle = 0 \\ \langle F_B^2 \rangle = \frac{2\xi(R)k_BT}{\Delta t} \end{cases} . \tag{1.16}$$

The value of the variance $\langle F_B^2 \rangle$ is determined as follows. In 3-D, consider the mean squared displacement of a single particle, over time scales such that the motion is over-damped and with external forces $F_C = 0$. The Langevin equation can then be discretized to obtain the mean-squared displacement after one time step:

$$\langle \Delta r^2 \rangle = d\langle F_B^2 \rangle \Delta t^2 / \xi^2 = 2dD\Delta t. \tag{1.17}$$

Thus Eq. (1.17) agrees with Eq. (1.13) if we choose $\langle F_B^2 \rangle = \frac{2\xi(R)k_BT}{\Delta t}$ in all dimensions.

In the over-damped limit, the net velocity of the particle can be solved simply:

$$\langle \vec{v} \rangle = \frac{\vec{F}_C}{\xi(R)}, \tag{1.18}$$

and the mobility is:

$$\mu = \frac{|\vec{F}_C|}{\xi(R)|\vec{E}|}. \tag{1.19}$$

Unfortunately, the sum of conservative forces $\vec{F}_C$ in electro-hydrodynamic is quite complicated. For instance, consider a particle which moves with a velocity $\vec{v}$. During its motion, the drag force due to the solvent slows it down. The drag force exerted by the fluid, and the force exerted by the particle on the fluid, are equal and opposite in direction. This produces a long-range flow when the particle is moving, and this will interact with other particles and walls. By generating and reacting to such fluid flows, particles experience hydrodynamic interactions with each other and with the walls. In computer simulations, the calculation of these hydrodynamic interactions is slow. The general approach taken here is treating everything as simple mechanical calculations. The efficiency of simulating the mechanical dynamics of particles is high compared to electro-hydrodynamics. Our first assumption is thus that, we neglect the hydrodynamic interactions.

Our second assumption in the project: Although the simulation particle occupies space, all forces are applied to its center of mass (CM). For a particle with a radius R, we thus assume that the field gradient over its size R is small:

$$\frac{R \cdot |\nabla \vec{E}|}{|\vec{E}_{CM}|} \ll 1. \tag{1.20}$$

As a result, the net force we use is an approximated force, and it cannot cause any rotation (since it is only acting on the CM).

In order to consider this point-like particle as a colloid that occupies space, the purely repulsive shifted Weeks-Chandler-Andersen (sWCA) potential is used to simulate its excluded volume:

$$\frac{U(r)}{4\epsilon} = \begin{cases} \left(\frac{\sigma}{r-r_{\text{off}}}\right)^{12} - \left(\frac{\sigma}{r-r_{\text{off}}}\right)^{6} + \frac{1}{4} & r < r_{\text{m}} \\ 0 & r \geq r_{\text{m}} \end{cases}, \tag{1.21}$$

where r is the distance between the wall and the CM of the particle, r_{off} is the offset corresponding to the hardcore component of the particle, ϵ measures the magnitude of the repulsive potential, and σ is the sWCA length-scale describing the extent of the soft potential. A particle thus has both a softcore and a hardcore. For simplicity, the magnitude of the repulsive potential is chosen to be the thermal energy of the solvent, $\epsilon = k_B T$. The sWCA potential is truncated at a distance $r_m = r_{\text{cut}} + r_{\text{off}}$ from the CM, where $r_{\text{cut}} = 2^{1/6}\sigma$ is the position of the minimum for the standard Lennard-Jones potential. The radius of the softcore is defined as the distance r_{cut} at which the particle starts to sense the sWCA potential. The radius of the hardcore is where $r = r_{\text{off}}$. However, we can define the particle nominal size as the position $r = r_{\text{off}} + \sigma$ for which $U(r) = k_B T$. Figure 1.2 provides an example of our sWCA potential.

Given a spherical particle of radius R_N, the average time for it to diffuse over a distance equal to its own size, τ_B is given by

$$\tau_B = \frac{R_N^2}{6D} = \frac{R_N^2 \xi(R_N)}{6 k_B T} = \frac{\pi \eta R_N^3}{k_B T}, \tag{1.22}$$

The time scale τ_B can be easily measured both in the labs and in the simulations, allowing for mapping our simulations onto a real case. For example, the HIV virus with a diameter of 100 nm has a diffusion coefficient $D = 2.2 \times 10^{-12}$ m^2/s at room temperature; its diffusion time is around 0.005 seconds.

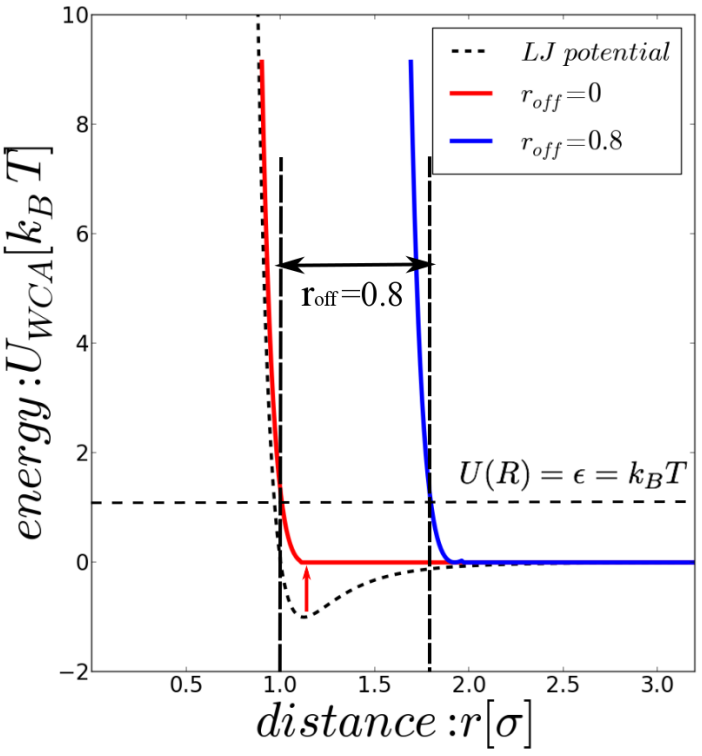

FIGURE 1.2: Examples of sWCA potential used to simulate the excluded volume of a particle with an offset $r_{off} = 0.8$. The LJ potential is cut at r_{cut} and shifted by ϵ vertically (red curve). Without changing the shape of the red curve, shifting it horizontally will add a hardcore to the same potential (blue curve).

Based on those assumptions and simulation methodologies, we can simulate the dynamics of particles that cannot be separated in free solution, allowing us to investigate different ways to achieve separation in a device and build a ratchet system.

1.2.4 Microfluidic devices

Microfluidic devices are wildly used in biophysics and biochemisty. The system we use is formed by a periodic series of deep wells and narrow channels, as Fig. 1.3 shows. This system was first introduced by Craighead, Han et al in 1999 [2]. Over the last 18 years, it has been tested for various applications. For instance, it has been used

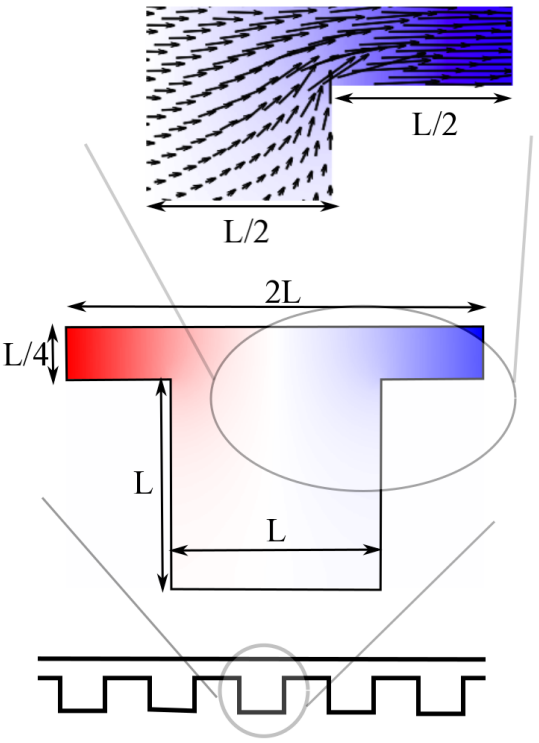

FIGURE 1.3: Diagram showing the cross-section of the microfluidic device introduced by Craighead and Han [2], and the field lines inside. The system is periodic in the direction from left to right, and the potential applied to the system is shown in color. The arrows indicate the direction and the amplitude of the electric field caused by the application of the electric potential.

for separating long DNA molecules and short rod-like molecules by electrophoresis [20–24].

Figure 1.3 shows the electrostatics of the device as computed using OpenFOAM [25], a software that is widely used to solve electromagnetic problems. The wells and channels are made of insulating material. When applying the electrical potential across the system, the distribution of electric field lines is non-uniform, and the sharp corners create huge field gradients. In our simulations, the CM of the particle does not experience such strong field gradients near the corners because of the steric interactions. Other details concerning the simulation and the scaling of the variable will be described in Chapter 2.

This microfluidic device provides the non-linearity we need because the field is not uniform. This provides one of the requirements for a ratchet process. However, we also need asymmetry.

Zero-integrated field electrophoresis, so-called ZIFE, is sometimes used in electrophoresis to separate molecules that have a field-dependent mobility from those who do not. As can be seen in Fig. 1.4, there are two duration t_+ and t_- and two field intensities E_+ and E_-. To satisfy the temporal asymmetry condition, the field cannot be symmetric in time; thus we must have $E_+ \neq E_-$. We must also satisfy the condition $E_+t_+ = -E_-t_-$, making the time-average field to be zero.

Obviously ZIFE can provide the symmetry-breaking feature to the system. Considering the nonlinearity of the microfluidic system mentioned before, the mean velocity of the particle will not generally be zero even through the mean field is zero.

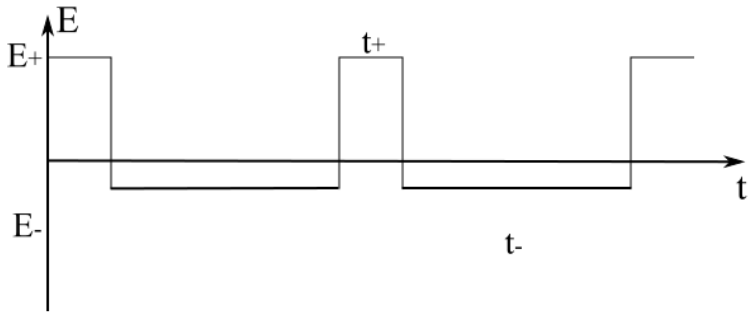

FIGURE 1.4: ZIFE pulse sequences: the magnitude and the direction of the electrical field satisfy the conditions $|E_+t_+| = |E_-t_-|$ and $E_+ \neq E_-$.

1.3 Swimming Cells

1.3.1 Motion of the active matter

The type of active matter we are interested in is swimming in a run and tumble fashion: a typical example is Escherichia coli (E. coli). As a living organism, E. coli requires oxygen, nutrition, and a suitable temperature to be functional; as long as such conditions are satisfied, E. coli can move, live and multiply forever. Using E. coli as an example, we can investigate the possibility for rectifying active matter in a ratchet system, and optimize the system to separate cells on the basis of size and/or swimming abilities. Robert Austin et al gave us a good example of this in a number of well-know papers [26, 27].

FIGURE 1.5: Schematic of active cells moving in a run and tumble fashion.

With a closer look at E. coli, one can recognize its rod-shaped body and tiny size. The length of this body is roughly 2-3 μm, and the diameter of the rod-shaped body is less than 1 μm. There are multiple

hair-like flagellums on the cylindrical structure, acting as locomotion and sensory organelles [5]. In general, an E. coli cell takes roughly one second to complete one "running" trajectory. Then it moves erratically for a short time, chooses a nearly random direction and "runs" again. This process is called "tumbling". During a run, it is common for E. coli to move at the rate of about 10 body lengths per second, roughly 20 to 30 μm, in the direction parallel to its cylindrical axis. After the run is completed, E.coli starts to rotate and move along the **same** direction with a velocity smaller than $6\mu m/s$, then choses a new, random direction; this "tumble" process takes roughly 0.1 second. Figure 1.5 shows a schematic of the Run/Tumble cell motion. By tracking the moving trace of E. coli, researchers have discovered that the running and tumbling times are distributed exponentially, while the velocities of runs and tumbles are distributed normally [5].

In an open system, the special run/tumble(R/T) motion of these swimmers is similar to Brownian motion: the mean velocity is expected to be zero in any dimension, while the mean square displacement is proportional to time t at long time.

Since this R/T motion is not in equilibrium, it has a preferred moving direction in a system with asymmetric geometries. The R/T movement is easy to simulate, but we need to make some assumptions to make sure our model is comparable to the real situation.

1.3.2 Assumptions and methods

I have had an opportunity to push a car to a gas station with my friends. It was the longest 20 minutes of my life. Our muscles were

able to push the car to move, but not strong enough to make it as fast as the engine does. The situation is very like the motion of the E. coli due to the random collision of the solvent molecules. At room temperature, the swimming velocity of E. coli can be 20 - 30 $\mu m/s$, while its diffusion coefficient is roughly $2 \times 10^{-13} m^2/s$ [5]. In one second, the distance that E. coli swims is 40 - 70 times larger than the distance due to the thermal noise. This leads to our first assumption in the project: we neglect the Brownian motion of E. coli. Thus the ballistic equation of motion is:

$$\vec{r}(t + \Delta t) = \vec{r}(t) + \vec{v}(t)\Delta t, \tag{1.23}$$

where $\vec{r}(t)$ is the position of the cell and $\vec{v}(t)$ is its velocity. The velocity $\vec{v}(t)$ depends on whether E. coli is running or tumbling. As mentioned before [5], the velocity is normally distributed, while the durations are exponentialy distributed. The question now is how to define these distributions.

Juan and his group have measured the velocity and duration of the E. coli run and tumble phases [28]. By statistical analysis they showed that the probability density function of both durations is of the form:

$$P(t) = \frac{1}{\tau} e^{-t/\tau}, \tag{1.24}$$

where τ is the average time duration of the "run" or "tumble" phase. The probability density function for the velocity was found to be of the form:

$$P(v) = \frac{1}{\gamma\sqrt{2\pi}} e^{-(v-\mu)^2/\gamma^2}, \tag{1.25}$$

where μ and γ are the parameters that characterize the normal distribution of the E. coli velocities. The results are shown in Table 1.1 and Fig. 1.6.

Parameters		
	Run	Tumble
Time (s)		
τ	1.2	0.1
Velocity($\mu m/s$)		
μ	37.84	5.99
γ	10.68	8.53

TABLE 1.1: Parameter values for the exponential distributions that best fit the run and tumble duration PDFs(Eq. (22)); Parameters for the Gaussian distributions that best fit the velocity PDFs (Eq. (23)) in the parallel direction. Cited from [28], print with permission.

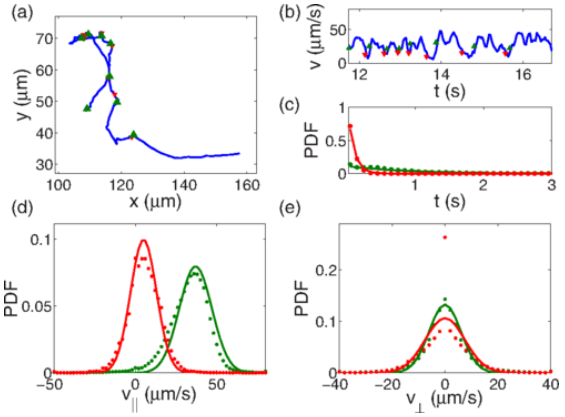

FIGURE 1.6: (a)A typical trajectory of an E coli cell. (b) The velocity for the trajectory in (a). (c) Duration PDFs (dots) and best fitting exponential distributions (solid lines) for runs (green) and tumbles (red). (d) Parallel velocity PDFs for runs (green dots) and tumbles (red dots), and the best fitting normal distributions (solid lines). (e) Same as in (d), but for perpendicular velocity. Cited from [28], print with permission.

For each R/T cycle, they studied the velocity components parallel $\vec{v}_{||}$ and perpendicular $\vec{v}_{\perp}$ to the net direction taken by the cell. One can notice that $\vec{v}_{\perp}$ is symmetrically distributed around a zero mean value. This suggests that a cell simply oscillates around its net moving direction during R/T motion. To simplify our simulations, we neglect the transverse fluctuation during the R/T motion.

In our simulation of R/T motion, for a given cell, its velocity is selected randomly and changed for every run or tumble phase; similarly, the duration of the run or tumble phase is selected randomly.

In every R/T cycle, the velocities and durations are generated following the normal and exponential distributions, as described by Eqs. (1.24) and (1.25). If we use the parameters Juan et al found in Table 1.1 and put those parameters into Eq. (1.24) and (1.25) to generate random velocities and durations, we are able to simulate the dynamics of one swimming cell. The cell's effective R/T mean free path (MFP) is then given by

$$\lambda = \mu_r \tau_r + \mu_t \tau_t, \tag{1.26}$$

where the subscripts r and t correspond to the run and tumble phases respectively. According to Table 1.1 the MFP of this cell is thus 46 μm. However this only represent one type of cell with one given MFP; in practice, we want to simulate swimming cells with **different** MFPs.

In order to simulate cells with different MFPs, we decided to vary the parameters of the distributions while keeping the parameter ratios equal to the values found in Table 1.1: μ_r/μ_t = 37.84 / 5.99, γ_r/γ_t = 10.68/8.53, τ_r/τ_t = 1.2/0.1. Finally, we neglect the contribution of the tumbling phase because it is negligible in Table 1.1 ($< 2\%$), so that Eq. (1.26) becomes

$$\lambda \cong \mu_r \tau_r. \tag{1.27}$$

We treated an E. coli cell as a spherical particle, following the run and tumble fashion described above. In order to simulate the dynamics of E. coli through a system of asymmetric walls, we must also simulate the interaction between a cell and a wall. Four different rules have been proposed to describe such interactions, as shown in Fig. 1.7.

These four rules were also discussed by Galajda et al [26, 27]. These authors showed that both rules (a) and (b) lead to the rectification of the cell R/T dynamics in asymmetric funnel structures. In this thesis, we choose the second rule to simulate the interaction between cells and walls.

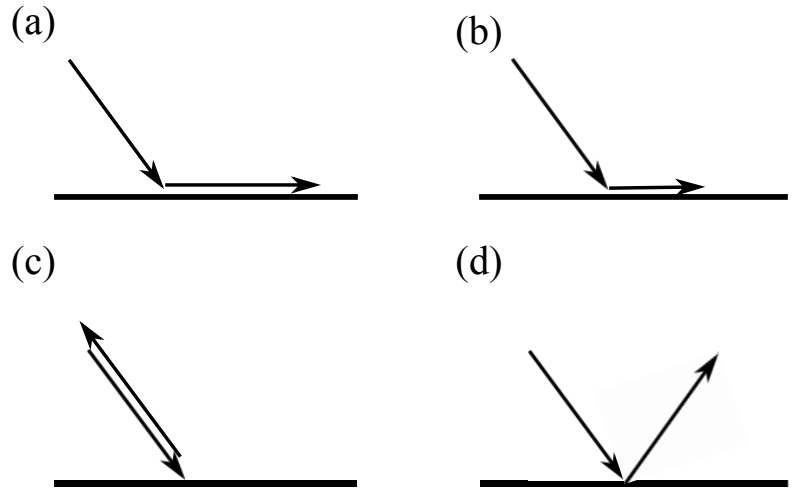

FIGURE 1.7: Four possible rules for wall-cell interactions. (a) The swimming cell realigns its velocity vector along the wall. (b) The cell keeps its original direction of motion so that only the component parallel to the wall leads to a net displacement (c) The active cell reverses its swimming motion upon touching the wall (d) The cell changes its direction of motion upon touching the wall; the new direction can be symmetric around the vertical direction or random.

For the second rule, when our cell hits the wall, its component of the driving force perpendicular to the wall plays no role since it is opposed by the repulsive force from the wall. Without reorientation of its driving force, the cell continues its motion along the wall with a velocity that corresponds to the component that is parallel to the wall. As a result, the velocities of sliding cells are smaller than when in free solution, as Fig. 1.7 (b) shows.

Bibliography

[1] Grossman, P. D., Colburn, J. C., *Capillary Electrophoresis, Theory and Practice*, Academic Press, 1992.

[2] Kirby, B. J., *Micro− and Nanoscale Fluid Mechanics*, Cambridge 2010.

[3] Heller, C., *Electrophoresis* 2001, *22*, 629-643.

[4] Manning, G. S., *Journal of Physical Chemistry* 1981, *85*, 1506-1515.

[5] Berg, H., *E. coli in Motion*, Springer, 2008.

[6] Squires, T. M., Quake, S. R., *Review of Modern Physics* 2005, *77*, 977-1026.

[7] Smoluchowski, M.v., *Experimentell nachweisbare, der ublichen Thermodynamik widersprechende Molekularphanomene, Physik. Zeitschr* 1912, *13*, 1069

[8] Feynman, R. P., Leighton, R.B., Sands, M., *The Feynman Lectures on Physics*, Addison-Wesley, 1963.

[9] Reimann, P., *Physics Report*, 2002, *361*, 57-265.

[10] Reuss, F.F., *Sur un nouvel effet de l'électricité galvanique* 1809, *2*, 327-337.

[11] Stellwagen, N., *Electrophoresis* 2009, *30*, S188-S195.

[12] Dorfman, K. D., King, S. B., Olson, D. W., Thomas, J. D. P., Tree, D. P., *Chemical Review*, 2013, *113(4)*, 2584-2667.

[13] Landers, J. P., *Capillary and Microchip Electrophoresis and Associated Microtechniques*, CRC Press, 2008.

[14] Li, T., Raizen, M., *Ann. Phys.*, 2013, *125*, 1.

[15] Smoluchowski, V., *Bull. Acad. Sci. Cracovie*, 1903, *3*, 182-200.

[16] Huckel, E., Die Kataphorese der Kugel, *Pgtsuj Z.*, 25, 204, 1924.

[17] Henry, D. C., *Proc. Roy. Soc. Lond.*, A133, 106, 1931.

[18] Coffey, W., Kalmykov, Y. P., Waldron, J. T., *The Langevin Equation*, World Scientific, River Edge 1996.

[19] Han. J., Craighead. H. G., *Science* 2000, *288(5468)*, 1026-1029.

[20] Laachi, N., Declet, C., Matson, C., Dorfman, K.D., *Phys. Rev. Lett.* 2007, *98*, 098106.

[21] Li, Z.R, Liu, G.R., Chen, Y.Z., Wang, J., Bow, H., Cheng, Y., Han, J., *Electrophoresis* 2008, *29*, 329-339.

[22] Han, J., Craighead, H. G., *Science* 2000, *288*, 1026.

[23] Fu, J., Yoo, J., Han, J., *Phys. Rev. Lett.* 2006, *97*, 018103.

[24] Kim, D., Bowman, C., Del Bonis-O'Donnell, J. T., Matzavinos, A., Stein, D., *Phys. Rev. Lett.* 2017, *188*, 048002.

[25] Weller, H. G., Tabor, G., Jasak, H., Fureby, C., *Comput. Phys.* 1998, *12*, 620-631.

[26] Galajda, P., Keymer, P., Chaikin, P., Austin, R., *Journal of Bacteriology* , 2007, *189*, 8704.

[27] Galajda, P., Keymer, P., Dalland, J., Park, S., Kou, S., Austin, R., *Journal of Modern Optics* , 2008, *55*, 3413.

[28] Sosa-Hernanadez, J., E., Santillan, M., Santana-Solano, J., *Phys Rev Lett E*, 2017, *95*, 032404.

Chapter 2

Electrophoretic ratcheting of spherical particles in simple microfluidic devices: making particles move against the direction of the net electric field

H. Y. Wang, H. de Haan, Gary W. Slater

To be submitted shortly to the *Journal of Chemical Physics*

Electrophoretic ratcheting of spherical particles in simple microfluidic devices: making particles move against the direction of the net electric field

H. Y. Wang, H. de Haan, Gary W. Slater

Department of Physics, University of Ottawa,
Ottawa, Ontario, K1N 6N5, Canada
Department of Physics, UOIT,
Oshawa, Ontario, L1H 7K4, Canada

May 11, 2018

Keywords:
Langevin Dynamics simulations; Computational modeling; Collid particles; electrophoresis; Ratchet effect

Abbreviations:

WCA	Weeks-Chandler-Andersen

Abstract

We examine the electrophoresis of spherical particles in microfluidic devices made of alternating wells and narrow channels, including a system previously used to separate DNA molecules. Our computer simulations predict that such systems can be used to separate spherical particles of different sizes that share the same free-solution mobility. Interestingly, the electrophoretic velocity shows an inversion as the field intensity is increased: while small particles have higher velocities at low field, the situation is reversed at high fields with the larger particles then moving faster. The resulting nonlinearity allows us to use asymmetric pulsed electric fields to build separation ratchets: particles then have a net size-dependent velocity in the presence of a zero-mean external field. Exploiting the inversion mentioned above, we show how to design pulsed field sequences that make a particle move against the mean field (an example of negative mobility). Finally, we demonstrate that it is possible to use pulsed fields to make particles of different sizes move in opposite directions even though their charge have the same sign.

1 Introduction

Separating particles and macromolecules is key to making progress in fields like chemical engineering and the biosciences. Electrophoresis [1–3], in its many forms, remains one of the most versatile methods to separate, analyze and purify charged analytes. Indeed, several new electrophoretic microfluidic devices have been proposed and built over the last decades [4]. One of them, shown schematically in Fig. 1a, has been used by Craighead et al [5] to separate long DNA molecules. Numerous theoretical studies have been published that can explain the subtle physical mechanisms at play when long DNA fragments (as well as short rod-like molecules [6, 7]) move between deep wells and narrow channels [8–10]. Our group has proposed to use asymmetric pulsed fields and/or an asymmetric well to design a DNA ratcheting system [11]. As far as we know, this has yet to be tested, except for short rods [12]. More recently, Cheng et al [13] simulated the motion of spherical particles of different sizes in the system shown in Fig. 1a. Interestingly, they found that the scaled electrophoretic

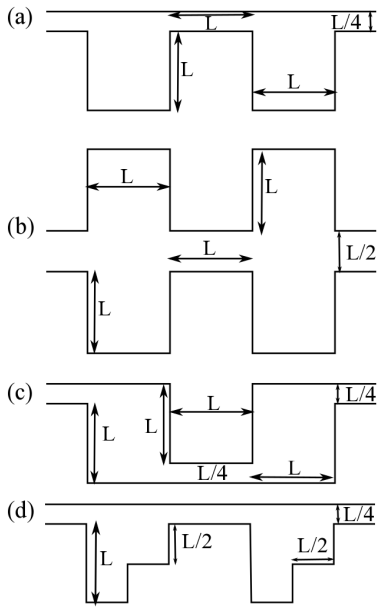

Figure 1: (a) The original system proposed by Craighead et al [5]: deep wells are connected by narrow channels (slits in a three-dimensional system). In our simulation system, the total length of one periodic unit is $L_{tot} = 2L$, the well depth is L and the channel height is $L/4$, as shown. (b) Similar to the previous system, except that we now have symmetry around the central plane leading to a channel height of $L/2$. (c) Zig-zag shaped device; here the length of the periodic unit is $L_{tot} = 4L$. (d) Similar to (a) above, except for the presence of a symmetry-breaking step inside the well.

mobility of large particles exceeds that of smaller particles if the electric field is high, but that the opposite is true at low field intensities.

In this paper we revisit the results of Cheng et al [13] and propose ways to build ratchet-like systems that exploit the nonlinearity of the underlying physical process. In order to do so, we will assume that we have spherical particles of different sizes that have the exact same mobility (in both sign and magnitude) in free-solution, making it impossible to separate them without using a sieve (such as a gel) or a specially designed microfluidic device. Although one can indeed use DC electric fields to separate these particles in the devices shown in Fig. 1, we will demonstrate that properly selected AC fields can allow us to manipulate particles in non-trivial ways, including making particles move against the net

field.

2 Method

We use Langevin Dynamics (LD) simulations [14] to study the motion of particles of different sizes in the devices shown in Fig. 1. The particles' properties are selected such that their velocity is size-independent in free solution (or equivalently between parallel walls). Since our proof of concept simulations do not include electrohydrodynamic effects, the application of an electric field on the charged particles is equivalent to applying a mechanical force. In a free solution with viscosity η, the velocity $\vec{v}(Q, R, \vec{E})$ of a spherical particle of size R and charge Q in an electric field $\vec{E}$ is then given:

$$\vec{v} = \frac{\vec{F}_E}{\xi} = \frac{Q\vec{E}}{6\pi\eta R}, \tag{1}$$

where $\vec{F}_E = Q\vec{E}$ is the force applied on the particle and $\xi = 6\pi\eta R$ is the friction coefficient. In order to obtain the same velocity for all particle sizes R we must choose $F_E(R) \propto Q(R) \propto R^1$. Obviously, this represents the most challenging situation for a separation device; other situations can be studied very easily.

The numerical simulations solve the LD equation of motion for the position $\vec{r}(t)$ of the particle [15]

$$m\ddot{\vec{r}} = \vec{F}_w + \vec{F}_E(R) - \xi(R)\dot{\vec{r}} + \vec{F}_B, \tag{2}$$

where m is the mass of the particle, $\vec{F}_w$ is the force between the particle and the walls, and $-\xi(R)\dot{\vec{r}}$ is the drag force. The Brownian force [15] $\vec{F}_B$ is taken as a Gaussian random variable with zero mean, $\langle \vec{F}_B \rangle = 0$, and variance $\langle F_B^2 \rangle = 2\xi k_B T/\Delta t$ in each dimension, where Δt is the simulation integration time step.

We use the shifted Weeks-Chandler-Andersen (sWCA) potential $U(r)$ to model the repulsive (steric) interactions between the walls and the particle:

$$\frac{U(r)}{4\epsilon} = \begin{cases} \left(\frac{\sigma}{r-r_{\text{off}}}\right)^{12} - \left(\frac{\sigma}{r-r_{\text{off}}}\right)^{6} + \frac{1}{4} & r < r_{\text{m}} \\ 0 & r \geq r_{\text{m}}, \end{cases} \tag{3}$$

where r is the distance between the wall and the centre-of-mass (CM) of the particle, r_{off} is the offset corresponding to the hard core component of the particle size, ϵ measures the magnitude of the repulsive potential, and σ is the sWCA length-scale describing the extent of the potential. The potential is truncated at a distance $r_m = r_{\text{cut}} + r_{\text{off}}$ from the CM, where $r_{\text{cut}} = 2^{1/6}\sigma$ is the position of the minimum for the standard Lennard-Jones potential. A particle thus has both a hardcore and a softcore and its nominal size is defined as the position $r = R$ where $U(R) = k_B T$; since we use a temperature $k_B T = \epsilon$, the nominal particle size is given by $R = r_{\text{off}} + \sigma$ and can thus be changed via the offset parameter $r_{\text{off}} \geq 0$.

In order to calculate the local electric force $\vec{F}_E(\vec{r})$, we must compute the field lines. First, an electric potential difference $\Delta\Phi$ is applied between the two ends of the periodic cell of the system. The field lines are then computed using OpenFOAM [16] (which is widely used to solve problems related to complex fluid flows, turbulence, heat transport, electromagnetics, etc.) assuming that the walls are perfect insulators. The resulting local field intensity is obviously much larger in the narrow channels, while the low field intensity at the bottom of the wells make the latter act as traps. The local field intensity $\vec{E}(\vec{r})$ is then tranformed into a local force $\vec{F}_E(\vec{r})$. Since only this electric force matters, we do not need to define the electric charge of the particles.

Because we must have $F_E \propto R$ in order to obtain a free-solution velocity that is independent of the particle size R, the electric force must scale like

$$\vec{F}_E(R, \vec{r}) = \left(\frac{R}{\sigma}\right) \vec{F}_E^{\sigma}(\vec{r}), \tag{4}$$

in our simulations, where F_E^{σ} is the force on the smallest particle (of radius $R = \sigma$) allowed in the simulation.

As mentioned above, the force $\vec{F}_E(\vec{r})$ is not uniform in space in our systems. In order to be able to compare the mobility of the particles in different systems, one must define a common measure of electric potential or effective field intensity. The effective intensity of the applied electric field will be defined as the force F_E^o that the smallest particle would feel in free-solution if we used the same potential difference. As a result, the effective electrophoretic mobility μ will be defined as the ratio between the time-averaged velocity of the particle, $\bar{v}$,

and the effective intensity of the applied electric force:

$$\mu = \frac{\bar{v}}{F_E^o}. \tag{5}$$

Each LD simulation is run until the particle has moved over at least 4000 periodic units of the device. We use two-dimensional simulations because the device geometries make the third dimension irrelevant. Lengths are measured in units of the sWCA lengthscale σ, forces in units of k_BT/σ, and times in units of the fundamental Brownian time $\tau \equiv \sigma^2/D_\sigma$, where D_σ is the diffusivity of the particle of size $R = \sigma$ in free solution. Therefore, the mobilities are measured in units of D_σ/k_BT. We chose $L = 20\sigma$ for our simulations; since the narrow channel has a width of $L/4$, the maximum particle radius is $R = 2.5\sigma$ for systems (a), (c) and (d), and 5σ for system (b). In the rest of this paper the units will not be included in order to be more concise.

3 Results: DC fields

3.1 Comparing the four different geometries

We first examine the performance of the four systems shown in Fig. 1 when a constant DC field is applied.

The system studied by Cheng et al. [13] is depicted in Fig. 1a. Our data (Fig. 2) show three regimes. The electrophoretic mobility is field-independent in both the low and high field regimes, but increases by a factor of $\approx 3-5$ in the intermediate field regime. The mobility is a strong function of the particle size in the low field regime; however, the size dependence is weaker for intermediate fields and negligible at high fields (the various lines then converge towards $\mu \approx 1$). Remarkably, the curves for the different particle sizes cross around the critical field $F_E^{o*} \approx 0.3$. Larger particles thus have lower mobilities at low fields but they are faster than the small particles when $F_E^o > F_E^{o*}$. Our results are fully consistent with those reported previously by Cheng et al. [13] (however, these authors did not observe

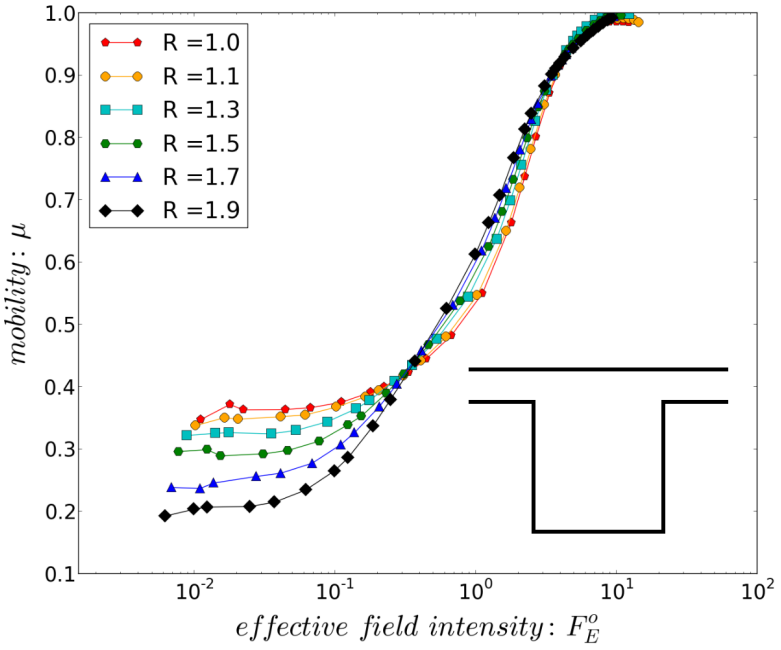

Figure 2: The electrophoretic mobility μ of spherical particles of radius R vs the effective field intensity F_E^o for the system shown in Fig. 1a.

the convergence at high fields because they limited their study to lower field intensities). The combination of the field-dependent mobility and the existence of the crossover point F_E^{o*} suggests that it is possible to build ratchet processes using this system, as we will show later.

Figure 3 shows the data for system (b) in Fig. 1. The results are similar, except for the fact that the low-field mobility is now a weak function of the particle size R. The mobility lines also converge at high fields, this time with a mobility that slightly exceeds unity, and the crossover field is smaller at $F_E^{o*} \approx 0.15$. However, the mobility is a slightly stronger function of the particle size in the intermediate regime; this makes system (b) a better choice than system (a) if DC fields are used.

Flipping every other well to create a zig-zag system that forces the particles to slalom, Fig. 1c, leads to major qualitative and quantitative differences (Fig. 4). While the mobilities are reduced by a factor of ≈ 2, the size-dependence of μ is increased for low fields. The

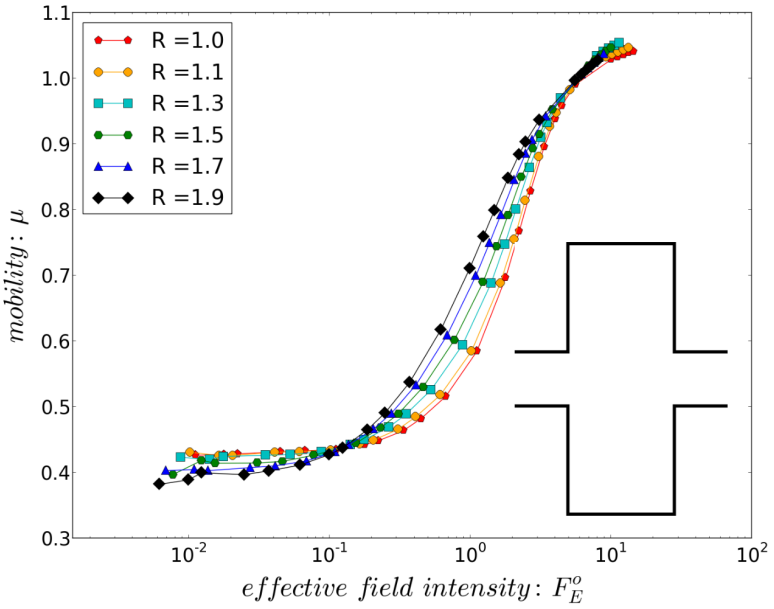

Figure 3: The electrophoretic mobility μ of spherical particles of radius R vs the effective field intensity F_E^o for the system shown in Fig. 1b.

crossover remains close to $F_E^{o*} \approx 0.3$, but $\mu(F_E^o)$ becomes a non-monotonic function of F_E^o at high fields. The weak size-dependence of $\mu(R)$ for $F_E^o > F_E^{o*}$ does not suggest that this system can be useful for separation purposes.

Since one of our goals is to propose ratchet designs, we also explore a system where a step inside the well breaks the left-right symmetry, Fig. 1d. Ratchets require nonlinearity (which we have for intermediate field intensities) and some asymmetry. The latter can be spatial, as in Fig. 1d, or temporal as we will propose later. As Fig. 5 shows, the mobilities are almost identical (although a bit higher at low fields) to what we observed for system (a). Unfortunately, the mobility is essentially identical whether the particles move from left-to-right or the opposite, with the former only slightly larger than the latter. Since entropy dominates at low field, it is not surprising that the mobility is then independent of the direction of the field. When the field intensity increases, the particles mostly follow the field lines and rarely visit the well, also leading to a mobility that barely changes with the field direction. This is quite different from what was observed for DNA molecules in

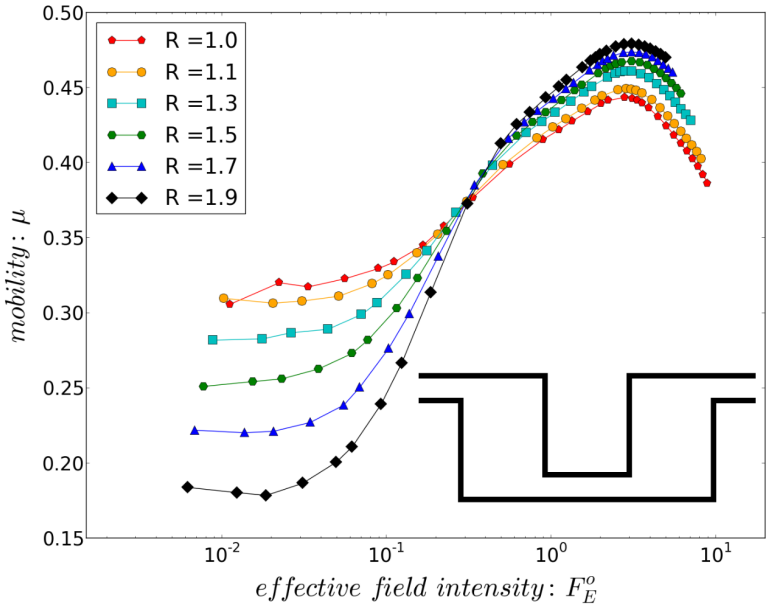

Figure 4: The electrophoretic mobility μ of spherical particles of radius R vs the effective field intensity F_E^o for the system shown in Fig. 1c.

ref [17]: in the case of flexible DNA molecules, the monomers follow different field lines and the non-uniform field leads to molecular deformations and highly asymmetric mobilities.

In short, the original system in Fig. 1a shows a size-dependent mobility for low and moderate fields, with a crossover at a critical field $F_E^{o*} \approx 0.3$. System (b) shows a mobility that has a stronger particle size dependence, but only for intermediate fields. The zig-zag system gives weaker size-dependent mobilities, while the results obtained for asymmetric system are not substantially different from those of the original system. Since system (a) is the simplest, both theoretically and experimentally, the rest of the paper will mostly focus on this geometry.

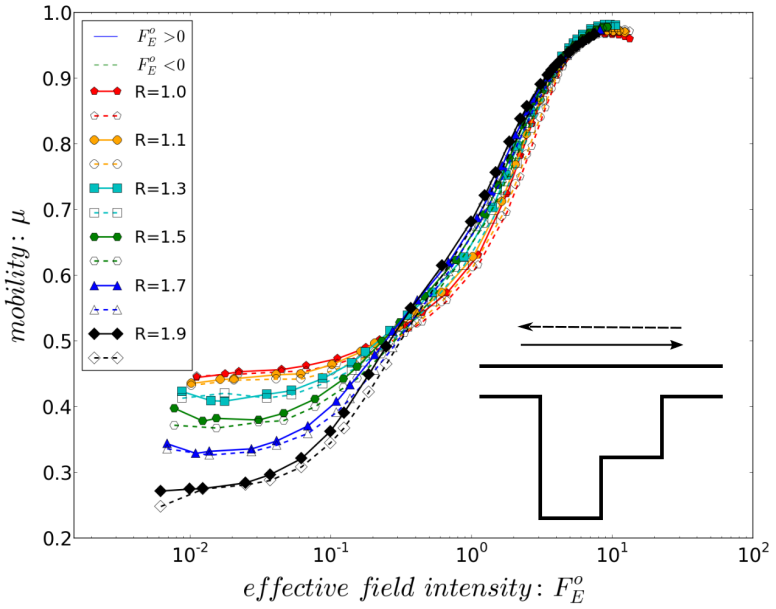

Figure 5: The electrophoretic mobility μ of spherical particles of radius R vs the effective field intensity F_E^o for the system shown in Fig. 1d.

3.2 Entropic effects and the low-field regime

In the low-field near-equilibrium regime, a particle samples all of the different parts of the system for equal amounts of time, i.e, entropy dominates. Figure 6a shows the probability $P_w(R)$ of finding the particle in the well during the simulation as a function of the field intensity for three different particle sizes; the corresponding mobility data are also given for comparison. Remarkably, the probability curves mirror the mobility curves and even cross at the same critical field $F_E^{o*} \approx 0.3$. The increase of the mobility at high fields is thus due to the fact that the particles then follow the field lines and rarely fall into the well (which acts as a trap because the field intensity is small in this region). The NW quadrant of Fig. 6b shows that the probability of presence is indeed uniform throughout the system at low field.

One can thus calculate the low-field probability $P_w^o(R)$ as the ratio of the well surface

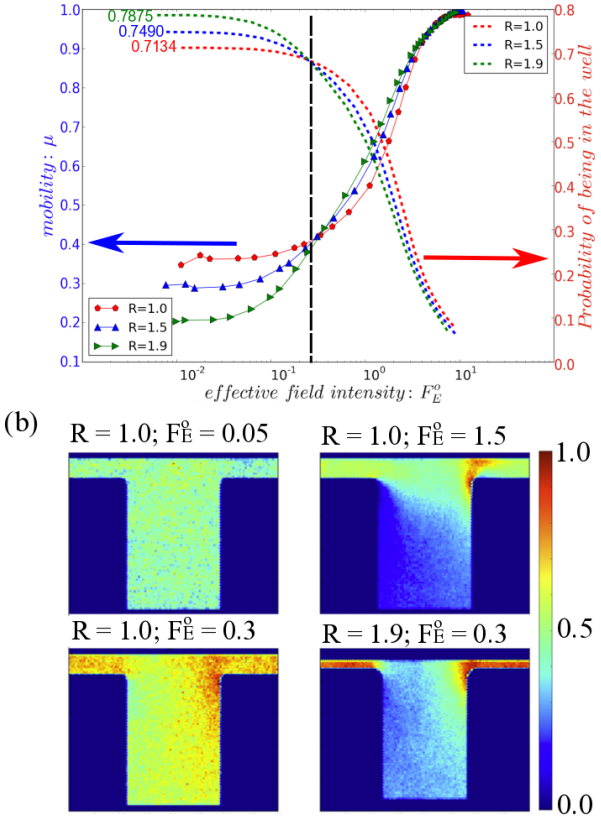

Figure 6: (a) Mobility μ (left y-axis) and probability of finding the particle in the well, P_w (right y-axis), for three different particle sizes R vs the effective field intensity F_E^o for the system shown in Fig. 1a. (b). Density plots showing the probability of finding the particles at different places inside the same system (warmer colours represent higher probability of occupying that position); four different cases are shown, with low, intermediate and high field intensities.

area available to the particle to the total surface area available in system (a):

$$P_w^o(R) = \frac{A_{well}(R)}{A_{total}(R)} = \frac{(L-R)(L-2R)}{\frac{3}{2}L^2 - 6LR + (2-\frac{\pi}{2})R^2}. \tag{6}$$

Table 1 gives the simulation low field plateau values obtained in Fig. 6a together with the theoretical values predicted using eq. (6). The agreement is excellent.

The fact that both $\mu(R)$ and $P_w^o(R)$ are field-independent at low field suggests there

R	$P_w^o(R)$: *theory*	$P_w^o(R)$: *simulation*
1.0	0.7118	0.7134(1)
1.5	0.7469	0.7490(2)
1.9	0.7847	0.7875(1)

Table 1: The low-field probability $P_w^o(R)$ of finding the particle in the well (from simulations and theory) for the three cases shown in Fig. 6a.

is a connection between them. The Ogston model [11] postulates that $\mu(R)$ should be proportional to the fractional surface area $\phi(R)$ accessible to a particle in a sieving system:

$$\mu(R) \propto \phi(R) = \frac{A_{total}(R)}{A_{total}(R=0)}. \tag{7}$$

Note that $A_{total}(R)$ is the surface area accessible to the particle when we take into account steric exclusion near the walls while $A_{total}(R=0)$ is the total area of the system. For system (a), this leads to:

$$\phi(R) = 1 - 4\left(\frac{R}{L}\right) + \left(\frac{4-\pi}{3}\right) \times \left(\frac{R}{L}\right)^2, \tag{8}$$

This relation works well for particles much smaller than the width of the narrow channel, $\frac{R}{L} < \frac{1}{8}$ (data not shown). However, eq. (8) fails for larger particles since it predicts that $\mu(R)$ should vanish when $\frac{R}{L} = (6 - \sqrt{24+3\pi})/(4-\pi) \approx 0.2546$ instead of $\frac{R}{L} = \frac{1}{8} = 0.125$. The reason for the failure of the Ogston model is due to the fact that in this limit, particle dynamics is entirely controlled by the difficulty of finding the channel by diffusion alone. The simplest way to improve (8) is to add an additional term

$$\phi^*(R) = 1 - 4\left(\frac{R}{L}\right) + \left(\frac{4-\pi}{3}\right)\left(\frac{R}{L}\right)^2 - \Omega\left(\frac{R}{L}\right)^3, \tag{9}$$

where $\Omega = \frac{8}{3}(100-\pi) \cong 258.29$ is needed if we impose $\mu(R = \frac{L}{8}) \propto \phi^*(R = \frac{L}{8}) = 0$. However, this value of lambda neglects the fact that we are using soft particles in our simulations (particles slightly larger than the nominal maximum size $R = \frac{L}{8} = 2.5$ can squeeze through the channel). We thus fitted the data using Ω as a free parameter and found that the optimal value was $\Omega \cong 230(5)$, which correspond to having a maximum particle size of $R_{max} \cong 2.57(2)$. Figure 7 shows the mobility data, this time rescaling the

mobility using $\phi^*(R)$. The low field mobility curves collapse perfectly, showing the validity of the modified Ogston concept that we proposed in eq. (9). Since $\phi^*(R=0)=1$, μ_{ϕ^*} is in a sense the mobility predicted for a point-like particle. For low field intensities, we can thus write:

$$\mu(R) \cong \mu_{\phi^*} \times \phi^*(R), \tag{10}$$

where $\mu_{\phi^*} \cong 0.47(3)$ for the case studied here.

We note that if we expand expression (9) about $R = R_{max}$ we obtain, to first order, $\phi^*(R) \propto \frac{R_{max}-R}{L}$, which is exactly the scaling that theory predicts for the diffusion coefficient of a point-like particle diffusing between cavities of size L if they are connected by holes of size $R_{max} - R$ [18]. Our extension of the Ogston theory is thus an interpolation between the two regimes predicted by theory for low field intensities.

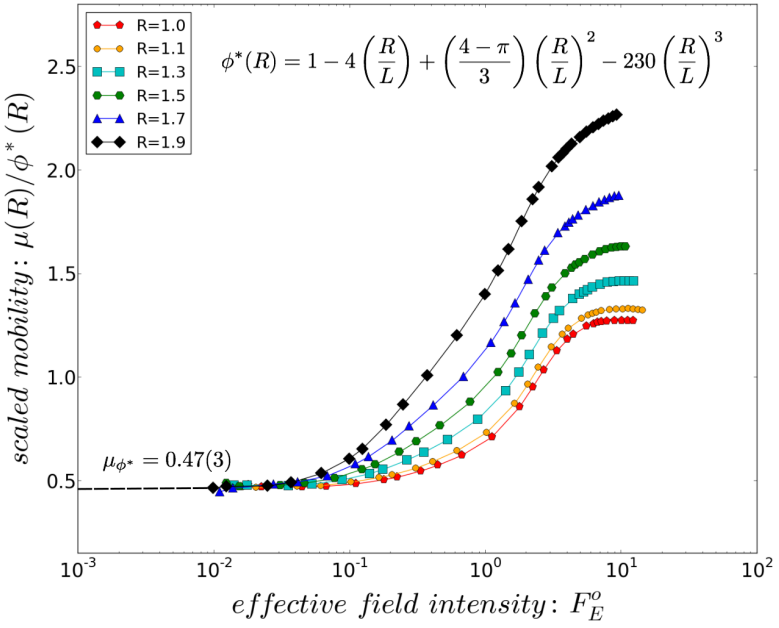

Figure 7: Scaled electrophoretic mobility $\mu(R)/\phi^*(R)$ of spherical particles of effective radius R vs the effective field intensity F_E^o for the system shown in Fig. 1a. The data collapse to the plateau value $\mu_{\phi^*} = 0.47(3)$.

3.3 High field intensities

As Fig. 6a shows, the probability for a particle to be trapped in low-field well regions decays rapidly for $F_E^o > F_E^{o*}$ and becomes negligible at high fields. This probability also becomes essentially independent of the particle size in this limit: the particles follow field lines and move from one narrow channel to the next without being affected by the well. In the intermediate field regime, small particles visit wells more frequently than large ones because the former have higher diffusion coefficients and thus change field lines more readily; this is why small particles are then slower than large ones.

Figure 6b nicely shows these differences between the three field regimes and the different particle sizes. While the particle visits all parts of the system at low field (NW quadrant), it spends very little time in the well at high field (NE). At the crossover point field F_E^{o*} the particle spends a fair amount of time moving from the well to the entrance of the next channel; a smaller particle (SW) goes deeper in the well than a larger one (SE), again explaining the inversion at the crossover field F_E^{o*}.

3.4 Empirical field dependence of the mobility

In order to optimize a separation system, it is often useful to have an empirical function that adequately describes the dependence of the mobility upon the experimental parameters. Our field data can be fitted using the empirical stretched exponential function

$$\mu(F_E^o) = \mu_\infty - \Delta\mu \ \times \ exp\left[-\left(\frac{F_E^o}{F_\alpha}\right)^\alpha\right]. \tag{11}$$

For system (a), we found that the high-field asymptotic mobility $\mu_\infty = 1.00 \pm 0.02$ for all particle sizes (data not shown). We thus fix $\mu_\infty = 1$ to reduce the number of fitting parameters; note that $\mu_\infty = 1$ is also the field-independent mobility of these particles at zero temperature (no diffusion; data not shown), as expected since they then follow the field lines. The low field plateau mobility is given by $\mu_\infty - \Delta\mu$, which we replace by $\mu_{\phi^*} \times \phi^*(R)$ as given by eq. (10), since this expression was shown to successfully explain the low mobility

data. We thus use only two free parameters (the stretched exponent $\alpha(R)$ and the critical field $F_\alpha(R)$) in order to fit the increase of the mobility when we go from the low to the high field regime.

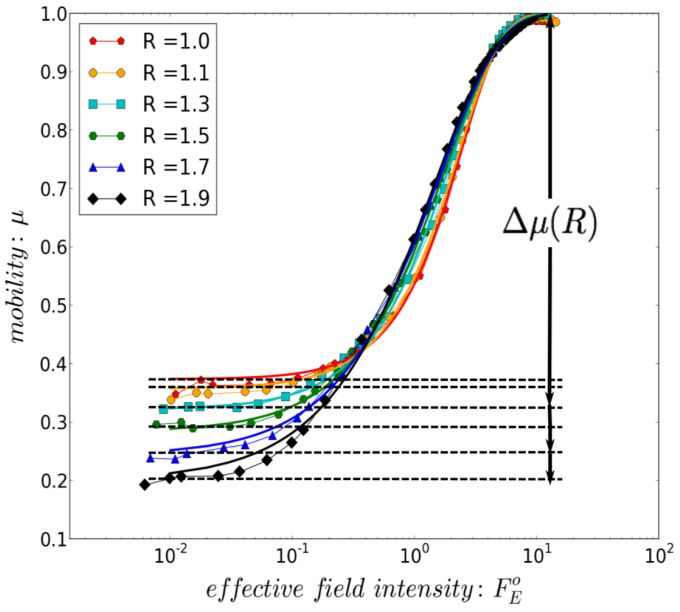

Figure 8: Fitting the mobility vs. F_E^o data for 6 different particle sizes R using eq. (11); the values of the fitting parameters are listed in Table 2.

As shown in Fig. 8, the fits are mostly excellent. Table 2 gives the value of the two fitting parameters for the six particle sizes (the mobility gap $\Delta\mu = 1 - \mu_{\phi^*}\phi^*(R)$ is also given for the sake of completeness). The two free parameters both decrease nonlinearly for larger particle sizes from their maximum values of $F_\alpha(1) = 2.41$ and $\alpha(1) = 1.26$ obtained for $R = 1$.

3.5 Geometry: device aspect ratios

Three lengths describe the system shown in Fig. 1a: the well depth and the channel length and height. Since only the aspect ratios matter, we keep the channel height constant and change (double) the other two dimensions. As Fig. 9 shows, deeper traps slow down the

R	$\Delta\mu(R) = 1 - \mu_{\phi^*}\phi^*(R)$	α	F_α
1.00	0.651	1.26	2.41
1.10	0.666	1.19	2.28
1.30	0.699	1.06	1.99
1.50	0.734	0.95	1.80
1.70	0.772	0.88	1.61
1.90	0.812	0.83	1.44

Table 2: The fitting parameters α and F_α defined in eq. (11). As described in the text, we fixed $\mu_\infty = 1$ and we used eq. (10) and the fact that $\Delta\mu(R) = 1 - \mu_{\phi^*}\phi^*(R)$.

particles while longer channels speed them up for the same potential difference. These effects do depend on particle size, smaller particles being more affected than larger ones because they visit the wells more frequently. Interestingly, the critical field $F_E^{o*} \approx 0.3$ is essentially unchanged (data not shown). Although these results imply that one can indeed tune the geometry in order to optimize the separation between two specific particles, it is generally more convenient to use a fixed system for a range of particle sizes. We will thus keep the original system aspect ratios for the rest of this paper.

4 Separation with a DC field

Two main methods are used to characterize the performance of separation devices [19]. First, it is useful to consider the quality of the "peak" (i.e., the spatial distribution of a single particle species) after a given experimental time t. This is defined as the dimensionless ratio of the mean distance travelled, $\bar{x}(t)$, to the standard-deviation $\sigma(t)$ of the distribution:

$$Q_x = \frac{\bar{x}(t)}{\sigma(t)} = \frac{\bar{v}t}{\sqrt{2Dt}} = \frac{\mu(F_E^o)F_E^o}{\sqrt{2D(F_E^o)}} \times \sqrt{t}, \tag{12}$$

where we explicitely included the fact that both the mobility μ and the dispersion coefficient D can be functions of the field intensity F_E^o in non-trivial systems. Simply said, Q_x measures

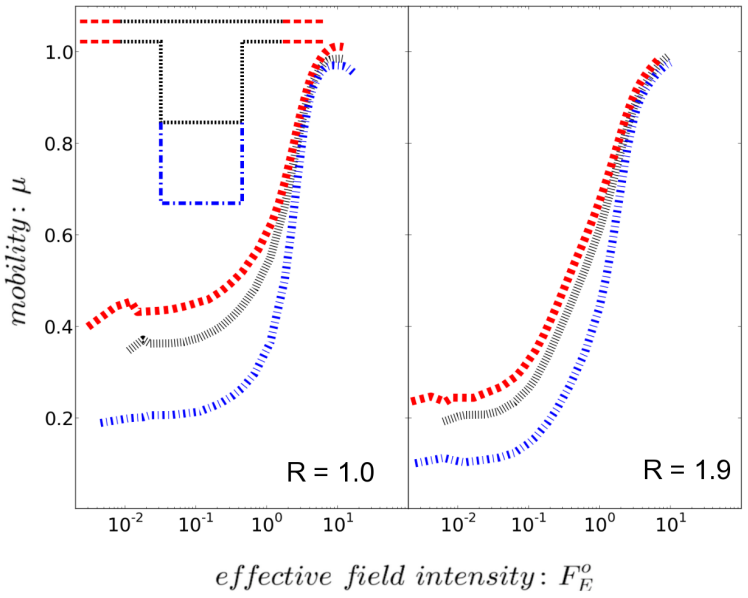

Figure 9: The electrophoretic mobility μ of spherical particles of radius R vs the effective field intensity F_E^o for the system shown in Fig. 1a and two different particle sizes R. Three different sets of aspect ratios are shown: the original one, one with channels twice as long, and one with a well twice as deep.

how tight the sample remains after moving over a mean distance $\bar{x}$ in a time t. Therefore, it measures the relative effects of drift and dispersion.

In free solution or between parallel walls, both μ and D are field-independent and we then obtain $Q_x \propto F_E^o\sqrt{R}$ since $D \propto 1/R$ (Stokes' law); the data in Fig. 10 confirm this prediction. Peak quality decreases substantially when the electrophoresis is carried out in system (a) instead; this is to be expected because dispersion always increases faster than peak spacing in non-uniform systems. As we can see, Q_x first increases slowly (sublinearly) with the field intensity up to about $F_E^o \approx 1$, and then rapidly (superlinearly) before it reaches a maximum value and starts decreasing for $F_E^o > 10$, which corresponds to the plateau regime $\mu = 1$ in Fig. 2. The rapidly increase near $F_E^o \approx 1$ may suggest it is the inflection point. The region over which we observe superlinear increase is that of the intermediate regime in Fig. 2; since the mobility is then a fairly strong function of the particle size R, this is likely

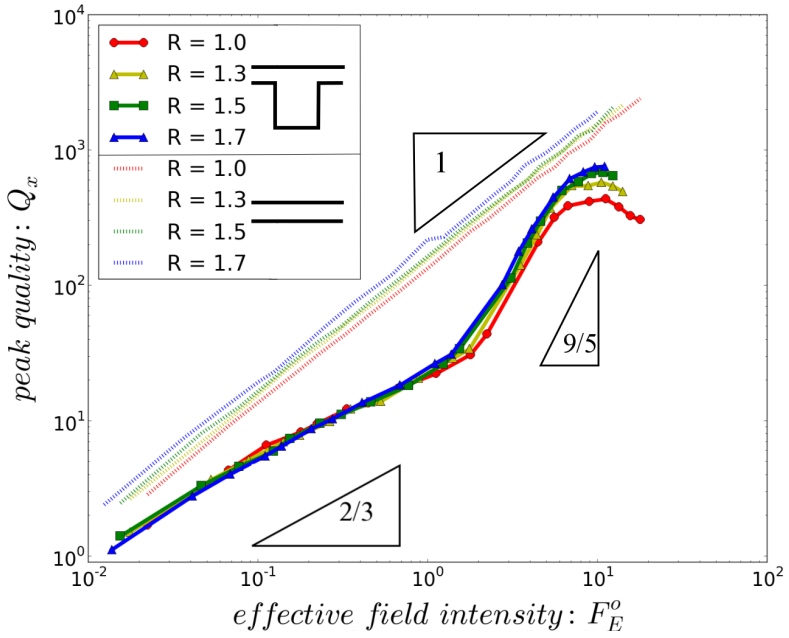

Figure 10: Peak quality, eq. (12), vs effective field intensity F_E^o for the system shown in Fig. 1a and four different particle sizes R. The result of simulations carried out between two flat walls are shown for comparison. The total simulation time for all particles is $t = 30,000$. The slope of 1 is predicted by theory; the other two slopes are only guides for the eye.

the best regime to use for separation purposes.

The second measure of performance is the resolution factor between two analytes (subscripts 1 and 2) [19]:

$$Re(t) = \frac{\bar{x}_1 - \bar{x}_2}{2\sigma_1 + 2\sigma_2} = \frac{(\bar{v}_1 - \bar{v}_2)t}{\sqrt{8D_1 t} + \sqrt{8D_2 t}} \propto \sqrt{t}. \tag{13}$$

Larger values of Re correspond to peaks that can more easily be distinguished. Figure 11 shows the time evolution of both the mean peak position $\bar{x}(t)$ and the resolution factor $Re(t)$ for two particles separated in systems (a) and (b) when we use a field intensity $F_E^o = 1.0$. As expected, $\bar{x}(t)$ increases linearly with time, while both the peak widths (the error bars) and the resolution factor $Re(t)$ increase like $\sqrt{t}$. We notice that system (b) provides better resolution than system (a) for a given time t, a result that we expected given the mobility curves that we presented in previous sections. As we can see, a value of $Re = 0.5$ corresponds

to two distinguishable populations. The best DC strategy is thus to use geometry (b) and the highest possible field intensity for which the mobility $\mu(R)$ remains strongly dependent on R.

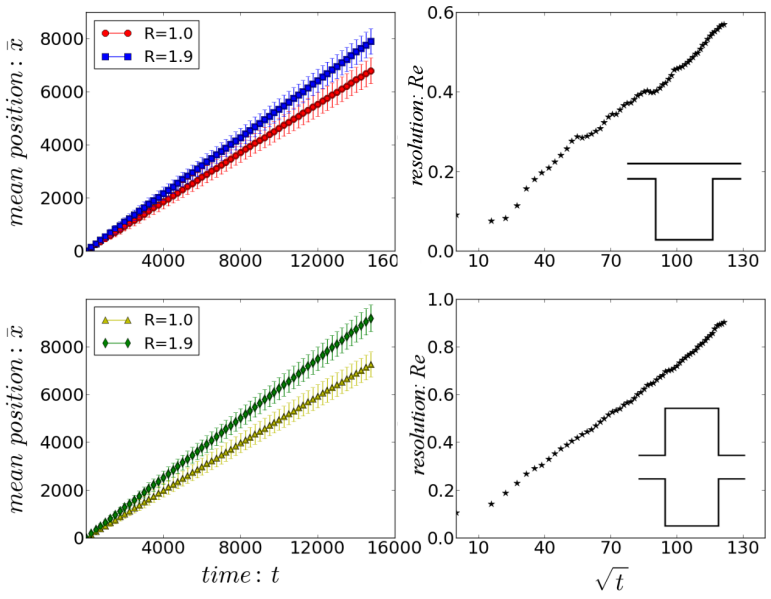

Figure 11: left: Time evolution of the mean position $\bar{x}(t)$ for particle sizes $R = 1.0$ and $R = 1.9$ in systems (a) and (b), under a field intensity $F_E^o = 1.0$. The error bars give the standard-deviation $\sigma(t)$. right: The corresponding time evolution of $Re(t)$.

5 Separation with pulsed fields: building ratchets

As mentioned previously, the nonlinearity of the system (the mobility is a function of the field intensity) and the fact that the mobility curves cross at some critical field F_E^{o*} open the door to the design of ratchet-like systems. For example, if the effective field F_E^o alternates between a high value $F_+ > F_E^{o*}$ in the positive direction and a low value $F_- < F_E^{o*}$ in the opposite direction, the particles will separate in both directions. Indeed, large particles move forward faster than small ones when $F_E = F_+$, while the opposite is true when $F_E = -F_-$.

Furthermore, the mean (or net) velocity $\bar{v}$ of a particle can be nonzero even when the mean field $\bar{F}_E$ is zero.

In order to examine these effects and propose interesting ideas for new devices, let's assume we use square pulses where $F_E = F_+$ for a time duration T_+ followed by $F_E = -F_-$ for a time duration T_-. The mean value of the field intensity is then simply:

$$\bar{F}_E = \frac{F_+T_+ - F_-T_-}{T_+ + T_-}. \tag{14}$$

As we will show, one can manipulate particles by properly choosing the field intensities and time durations.

If both T_- and T_+ are large compare to the times required to go from one well to the next, we basically have a DC field in both directions and we predict

$$\bar{v}(R) = \frac{\mu(F_+, R)F_+T_+ - \mu(F_-, R)F_-T_-}{T_- + T_+} \quad (T_\pm \to \infty). \tag{15}$$

For short pulses, however, the particle simply feels the mean value of the field and we expect

$$\bar{v}(R) = \mu(\bar{F}_E, R) \times \bar{F}_E \qquad (T_\pm \to 0). \tag{16}$$

Although a zero-mean field $\bar{F}_E = 0$ implies $\bar{v}(R) = 0$ at high frequency, we actually expect $\bar{v}(R) > 0$ at low frequency. The latter is an example of a ratchet.

Studying the full electrophoretic phase diagram as a function of the four pulse parameters is beyond the scope of this article. As an illustrative example using the system of Fig. 1a and the DC data of Fig. 2, let us consider the following forward pulse conditions: $F_+ = 1 > F_E^{o*}$ (high field with good size separation under DC conditions) and $T_+ = 200$ (long enough for our particles to travel over at least two wells). The chosen reverse field $F_- = 0.1 < F_E^{o*}$ provides decent particle separation in DC conditions. Since $\mu(F_- = 0.1) \approx 0.3$, a time of $T_- \approx 1300$ is required to cross a single system cell. We thus vary T_- between 1 to 8000 in order to explore a wide range of mean field intensities $\bar{F}_E(T_-)$, and we note that $\bar{F}_E = 0$ when $T_- = 2000$. Figure 12 shows the net velocity $\bar{v}(\bar{F}_E)$ as we vary T_-. All particles have a non-zero ratchet velocity when $\bar{F}_E = 0$ because of the nonlinear properties of the system. More interesting perhaps is the situation at $\bar{F}_E \approx -0.04$

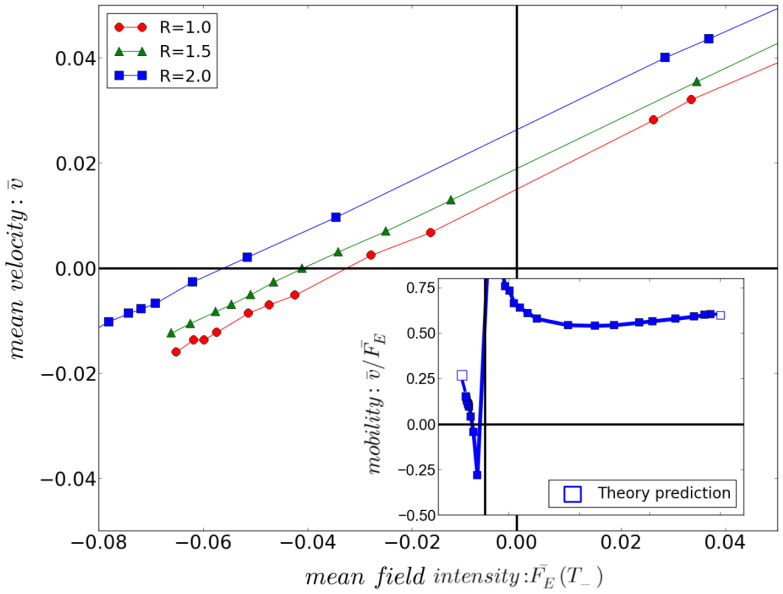

Figure 12: Mean velocity $\bar{v}$ vs. mean field intensity $\bar{F}_E(T_-)$ for three particle sizes R under pulsed field conditions. The field alternates between a value of $F_+ = 1$ for a duration $T_+ = 200$ and a value of $F_- = -0.1$ for a variable time duration T_-; the value of the corresponding mean field $\bar{F}_E(T_-)$ is obtained using eq. (14). Inset: The effective mobility ratio $\bar{v}/\bar{F}_E$ vs $\bar{F}_E(T_-)$ for the particle of size $R = 2.0$. The two empty symbols indicate the predicted values in the two extreme cases $T_- \to 0$ and $T_- \to \infty$, which are equivalent to using DC fields of intensities 1.0 and 0.1, respectively.

(corresponding to $T_- \approx 3467$): the large $R = 2$ particle then has a positive net velocity, while the small $R = 1$ particle moves in the opposite direction and the mid-size $R = 1.5$ particle has a negligible net velocity. These curves show that by properly choosing the pulse conditions, one can manipulate the net velocity of the particles basically at will. The inset shows the effective mobility $\bar{v}/\bar{F}_E$ for the $R = 2$ particle. The mobility diverges at the origin because the particle has a non-zero velocity when $\bar{F}_E = 0$. There is a narrow regime of pulse conditions where the particle moves against the direction of the mean applied field (i.e., $\mu < 0$); this is an example of absolute negative mobility, a phenomenon previously reported by several groups [20–22].

Figure 13 shows the time evolution of the separation between two different particles under pulsed and DC field conditions with the same mean field intensity. The two simulations were carried out until a similar resolution $Re \simeq 0.7$ was achieved (we note that $Re(t) \propto \sqrt{t}$ in both cases, as expected). Not surprisingly, the pulsed field system requires much longer durations (about 10 times longer). However, the two particles move in opposite directions under these pulsed field conditions because the smaller one is in a regime of absolute negative mobility; this should make it possible to capture and manipulate them more easily. In order to achieve this separation, the DC system has to be of a length of at least 7200 here since this is the distance travelled by the fastest particle ($R = 1.4$). Interestingly, the pulsed field system can be as small as 3000, the final distance between the two bead populations. Those results are typical of this kind of systems: ratchet pulse conditions are slower, require smaller footprints and allow one to move particles having the same free-solution mobility in opposite directions.

Figure 14 shows another separation strategy. We use pulsed conditions P_1 for $t < 118,260$ and a different set P_2 for longer times. As we can see, P_1 was chosen so that the two smallest particles have low velocities (the smallest one actually going backward); the large $R = 2.2$ particles are thus moving away from the rest and can be collected at position $x \approx 2000$ in the device. Conditions P_2 are chosen to launch the $R = 1.5$ particles; note that the smaller particles retain a negligible velocity during P_2. After a time $\approx 4 \times 10^5$, the $R = 1.5$ particles reach position $x = 2000$ and can also be captured. In order to capture the remaining $R = 1.0$ particles, one would have to switch to a final set of pulsed conditions although by then a DC field should be used for more efficiency. This is just one example where one could use pulsed fields and ratchet effects to move particles at will and potentially extract selected ones from a mixture.

6 Conclusion

Inspired by the results of Cheng et al [13], we have used computer simulations to investigate the electrophoretic motion of charged particles in multiple geometries and under various field

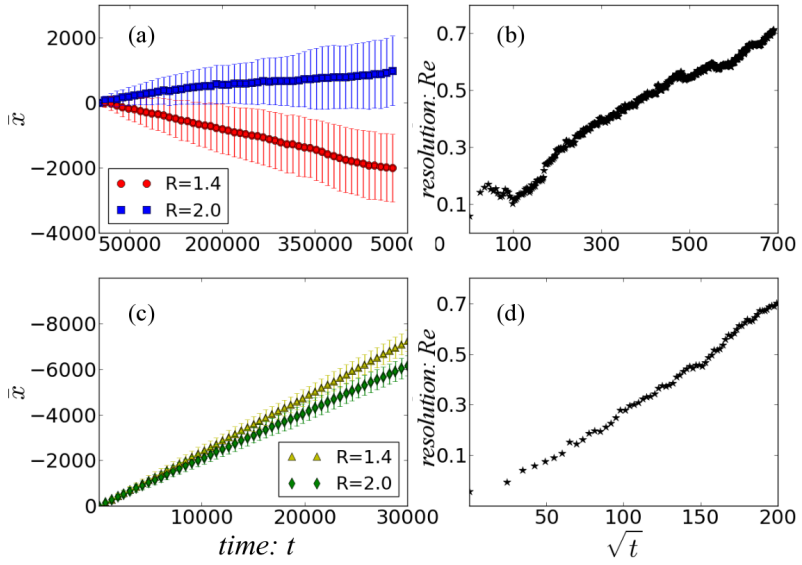

Figure 13: Separation of particles of size $R = 1.4$ and $R = 2.0$ using pulsed (a and b) and DC (c and d) fields. The pulse parameters are $F_- = -0.1$, $F_+ = 1$, $T_- = 9120$, and $T_+ = 480$, for a mean field intensity of $\bar{F}_E = -0.045$. The DC field intensity is $F_E^o = -0.045$. (a) Mean displacement $\bar{x}(t)$ vs time t for pulsed fields; the bars represent the standard deviation of the particles distributions. (b) The resolution factor $Re(t)$ corresponding to the data in (a). (c) Mean displacement $\bar{x}(t)$ vs time t when a DC field is used. (d) The resolution factor $Re(t)$ corresponding to the data in (c).

conditions. We have proposed an Ogston-like theory to explain the size-dependence of the particle mobilities in the low-field regime, as well as a simple empirical stretched exponential function to describe the field dependence of the mobility. In the intermediate regime, the distributions of particles remain tight during migration while their mobilities show a useful size-dependence.

Based on these results, we have shown that it is possible to produce ratchet-like effects in such systems in order to manipulate particles in non-trivial ways. These ratchet effects take advantage of the nonlinearity of the system and, in some cases, of the mobility crossover observed for intermediate field intensities. Since a geometrically asymmetric system appears to be inefficient because the particles tend to follow field lines in the useful regime, we have

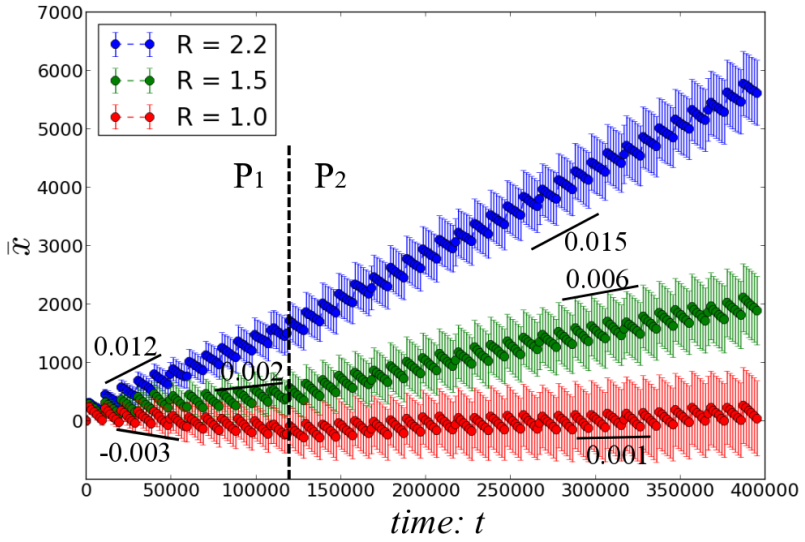

Figure 14: Time evolution of the mean position $\bar{x}(t)$ of particles of sizes $R = 1.0$, $R = 1.5$ and $R = 2.2$ in system (a) under pulsed field conditions. The error bars give the standard-deviation $\sigma(t)$. For the first 12 pulse cycles ($0 \leq t \leq 118,260$) the pulsed field conditions are P_1=($F_- =$ -0.1; $F_+ = 1$; $T_- = 9360$; $T_+ = 495$). For longer times the pulsed field conditions are P_2=($F_- =$ -0.1; $F_+ = 1$; $T_- = 9360$; $T_+ = 555$).

shown that asymmetric pulsed fields can be used to break the symmetry and obtain ratchet effects, including absolute negative mobilities.

Although we should not neglect the fact that pulsed field separations are usually substantially slower than separations that use simple DC fields, there are many advantages to employing pulsed fields in some cases. For instance, we showed that when properly designed, such separations require smaller footprints (shorter systems) and may even force similarly charged particles to move in opposite directions. It is even possible to launch one species at a time from mixture, a nice feature that could potentially be exploited to purify samples.

It would be interesting to expand the work presented here to the case of non-spherical particles (such as rods) because field reversal may force an analyte to rotate, thus adding a fundamental time scale that could be exploited using pulsed fields, just like the relaxation times of flexible polymers in gels and microfluidic systems. [4]

Acknowledgments: The LD simulations were performed with the ESPResSo package on the computing resources provided by SHARCNET and Compute Canada. We also acknowledge the support of the Natural Sciences and Engineering Research Council of Canada (NSERC), funding reference number RGPIN/046434-2013.

References

[1] Grossman, P. D., Colburn, J. C., *Capillary Electrophoresis, Theory and Practice*, Academic Press 1992.

[2] Kirby, B. J., *Micro− and Nanoscale Fluid Mechanics*, Cambridge 2010.

[3] Heller, C., *Electrophoresis* 2001, *22*, 629-643.

[4] Dorfman, K. D., King, S. B., Olson, D. W., Thomas, J. D. P., Tree, D. R., *Chemical. Reviews* 2013, *113*, 2584-2667.

[5] Han. J., Craighead. H. G., *Science* 2000, *288(5468)*, 1026-1029.

[6] Laachi, N., Declet, C., Matson, C., Dorfman, K.D., *Phys. Rev. Lett.* 2007, *98*, 098106.

[7] Li, Z.R, Liu, G.R., Chen, Y.Z., Wang, J., Bow, H., Cheng, Y., Han, J., *Electrophoresis* 2008, *29*, 329-339.

[8] Han, J., Craighead, H. G., *Science* 2000, *288*, 1026.

[9] Fu, J., Yoo, J., Han, J., *Phys. Rev. Lett.* 2006, *97*, 018103.

[10] Kim, D., Bowman, C., Del Bonis-O'Donnell, J. T., Matzavinos, A., Stein, D., *Phys. Rev. Lett.* 2017, *188*, 048002.

[11] Tessier, F., Slater G. W., *Applied. Phys. A.* 2002, *75*, 285-291.

[12] Li, Z.R., Liu, G.R., Han, J., Chen, Y. Z., *Anal. Bioanal. Chem.* 2009, *394*, 427-435.

[13] Cheng, K. L., Sheng, Y. J., Jiang, S., Tsao, H. K., *J. Chem. Phys.* 2008, *128*, 101101.

[14] Grest, G. S., Kremer, K., *Phys. Rev. A.* 1986, 33, *3628-3631.*

[15] Coffey, W., Kalmykov, Y. P., Waldron, J. T., *The Langevin Equation*, World Scientific, River Edge 1996.

[16] Weller, H. G., Tabor, G., Jasak, H., Fureby, C., *Comput. Phys.* 1998, *12*, 620-631.

[17] Tessier, F., Labrie, J., Slater, G. W., *Macromolecules* 2002, *35*, 4791-4800.

[18] Berezhkovskii, A. Zitserman. V., Shvartsman. S. *J. Chem. Phys.* 2003, *119*, 6991-6993.

[19] Giddings, J.C., *Unified Separation Science*, New York: Wiley 1991.

[20] Slater, W. G., Guo, H. L., Nixon, G. I., *Phys. Rev. Lett.* 1997, *78*, 1170-1173.

[21] Hanggi, P., Marchesoni, F., *Rev. Modern. Phys.* 2009, *81*, 387-442.

[22] Ros, A., Eichhorn, R., Regtmeier, J., Duong, T. T., Reimann, P., Anselmetti, D., *Nature* 2009, *436*, 928.

Chapter 3

Additional results for Chapter 2

3.1 Simulation units

It is possible to estimate the scale our simulation dimensionless parameters by comparing to an experimental system. In ref. [1], the width of the channel is $\sim$ 50 nm; since our channel widths are 5 σ, our unit of length is 1 σ = 10 nm. If we assume that a charged particle carries a charge of 100 e, where e is the elementary charge, and that it is driven by electrical fields that vary from 20 to 200 V/cm, the colloid is driven by an electric force in the range of 10^{-13} to 10^{-12} N. On the other hand, our simulation force is of order k_BT/σ, which is in the same range ($\sim$ 10^{-12} N).

3.2 Ratchet application

In the previous Chapter, we investigated the possibility of using DC and pulsed electric fields to manipulate charged particles in a microfluidic system. The purpose of this short chapter is to supplement the investigation of asymmetric pulse fields and ratchet effects.

Separating charged particles in a temporal asymmetric ratchet system is like making an elephant dance: slow, but possible. In Chapter 2, we demonstrated that we can separate two particles in opposite directions; we also showed that launching particles one species at a time from a mixture is possible. Here we determine how

we can make one specific particle stay at the origin and everyone else move away by using asymmetric pulsed fields.

In the limit of short pulses, particles are driven by the mean electric field. This does not allow us to affect different particles in different ways. We thus assume that the pulses have long durations compared to the time required to move between two wells. At $t = 0$, all particles are in the same chamber of the system. Suppose that we would like to make the smallest particle (radius R_s) completely backtracks to the origin at the end of each pulse cycle. This requires that $\bar{v}(R_s) = 0$ or, solving Eq. 15 from Chapter 2:

$$\mu(R_s, F_+)T_+F_+ = \mu(R_s, F_-)T_-F_-. \tag{3.1}$$

Equation (3.1) can be rewritten as:

$$\frac{T_-}{T_+} = \frac{\mu(R_s, F_+)}{\mu(R_s, F_-)}\frac{F_+}{F_-}. \tag{3.2}$$

Once the magnitudes F_+ and F_- are chosen, the ratio $\frac{\mu(R_s,F_+)}{\mu(R_s,F_-)}$ can be computed for the smallest particle and Eq. (3.2) then gives the time ratio that makes the smallest particle stay at the origin. For a particle with a radius R_i, the mean velocity is simply:

$$\bar{v}(R_i) = \frac{F_+T_+\mu(R_i, F_+) - F_-T_-\mu(R_i, F_-)}{T_+ + T_-}. \tag{3.3}$$

Using Eq. (3.2), the mean velocity of the particle is:

$$\bar{v}(R_i) = \left[(\mu(R_i, F_+) - \frac{\mu(R_s, F_+)}{\mu(R_s, F_-)}\mu(R_i, F_-)\right]\frac{F_+}{1 + T_-/T_+}. \tag{3.4}$$

Given the field intensities F_+ and F_-, and the ratio $\frac{\mu(R_s,F_+)}{\mu(R_s,F_-)}$, the smallest particle has $\bar{v}(R_s) = 0$. For other particles, the mean velocity depends on $\mu(R_i, F_-)$ and $\mu(R_i, F_+)$, such that $\bar{v}(R_i)$ is a function of the particle size R_i.

Let's choose the smallest particle to be of size $R_s = 1.0$, and the forces F_+ and F_- to be 1.5 and 0.3, respectively. The crossover field $F_- = F_E^{o*}$ implies that all particles move backward at the same velocity $v_- = \mu(F_E^{o*})F_E^{o*}$.

There are two advantages to choosing $F_- = F_E^{o*}$: the first one is time-efficiency, the second is the quality of the separation. Time-efficiency requires the velocity of the particle to be as large as possible. Figure 2 in Chapter 2 shows that the mobility μ increases with the effective field intensity F_E; we thus need a larger F_- to make the particle backtrack faster, hence small values of T_- are needed. Separation partly relies on the quality of the peak Q_x; Fig. 10 in Chapter 2 shows that peak quality Q_x is increasing with the field intensity. A larger F_- produces better peak quality, thus making it easier to distinguish the peaks. In addition, separation also relies on the mean velocity difference, as Eq. 13 showed in Chapter 2. If the sign of the mean velocity difference is negative during T_- (which would be the case if $F_- < F_E^{o*}$ were chosen), we lose some of separation. As a conclusion, the best strategy for choosing F_- is thus to make it equal to F_E^{o*} for which the mobility is relatively high yet the same for all species.

For $F_+ = 1.5$, $F_- = 0.3$, and $R_s = 1.0$, the mobilities are $\mu(F_+) \cong 0.62$ and $\mu(F_-) \cong 0.43$, and according to Eq. (3.2), we need a time ratio $\frac{T_-}{T_+} \cong 7.2$ for this particle to have a zero net velocity. When $F_+ = 1.5$, the time required for the R_s particle to travel one chamber is $2L/(\mu(1.5) \cdot 1.5) \cong 97$. We need this particle to pass through multiple chambers during one long pulse cycle; therefore, we chose $T_+ = 700$.

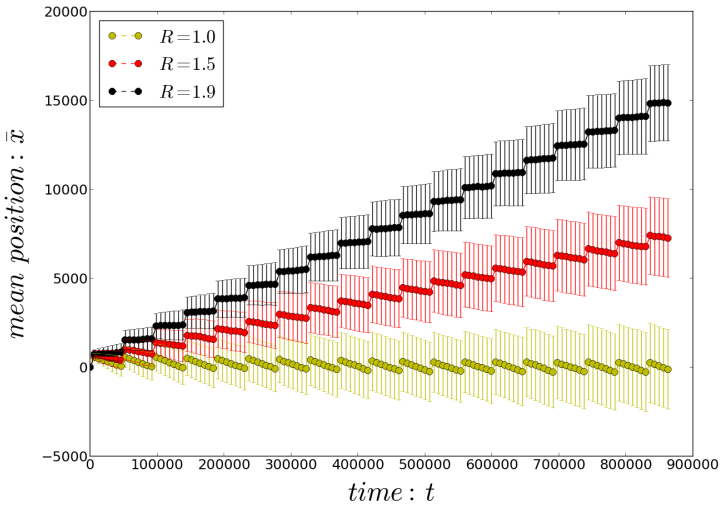

FIGURE 3.1: Time evolution of the mean position $\bar{x}(t)$ of particles of sizes R = 1.0, R = 1.5 and R = 1.9 in system (a) under pulsed field conditions. The error bars give the standard- deviation $\sigma(t)$. For the 150 pulse cycles ($0 \leqslant$ t $\leqslant$ 861,000), the pulsed field conditions are $F_- = 0.3$; $F_+ = 1.5$; $T_- = 5040$; $T_+ = 700$. The mean field is $\bar{F} \cong 0.446$.

Figure 3.1 meets our expectations: during the 150 pulse cycles, the smallest particle oscillates around the origin, while the other particles are moving at different mean velocities. Obviously, it is possible to make the R_s =1.5 particle stay at the origin instead. For particles with a radius smaller than 1.5, the net displacement would then be negative; while for particles with a radius larger than 1.5, their motion would be along the positive direction. Using such an approach, one can design pulse sequences to manipulate particles at will.

Bibliography

[1] Han, J., Fu, J., Schoch, R. B., *Lab on a Chip* 2008, *8*, 23-33.

Chapter 4

Rectifying the motion of self-propelled bacteria using funnels: a coarse-grained model for sedimentation and migration

H. Y. Wang, Gary W. Slater

Manuscript to be submitted for publication.

Rectifying the motion of self-propelled bacteria using funnels: a coarse-grained model for sedimentation and migration

H. Y. Wang, Gary W. Slater

Department of Physics, University of Ottawa,
Ottawa, Ontario, K1N 6N5, Canada

May 11, 2018

Keywords:

Ratchet effects; Computational modeling;
Active matter; Biased Random Walks

Abbreviations:

WCA	Weeks-Chandler-Andersen
1DLBRW	one-dimensional lattice biased random walk
MFP	mean free path

Abstract

Rectification of motile E. coli bacteria has been observed when confined in a closed environment partitioned using porous walls with funnel shaped channels. We simulate this ratchet process using a simple mechanical model that includes some details of the cells run/tumble process. In an open system, it is possible to define a velocity and a diffusion coefficient for the cells, while dynamics in a closed system is equivalent to sedimentation. We show that the performance of the ratchet can be linked to the value of a Peclet number, like in separation science. We further demonstrate that the dynamics can be mapped onto a simple Lattice Biased Random Walk with only three variables. We identify the link between these coarse-grained variables and some geometric and cell parameters. Our approach can be used to optimize the system in order to separate cells on the basis of their swimming abilities.

1 Introduction

Asymmetric boundaries cannot rectify the motion of randomly moving objects in thermodynamic equilibrium. However, a non-equilibrium component, such as a zero-mean alternating field or non-Brownian random motion, can lead to net displacements even if there is no net driving force. A nice example was recently reported by Galajda et al: a population of self-propelled randomly swimming bacterial cells was shown to accumulate on one side of a porous membrane with funnel-shaped channels [1,2]. The unique run/tumble (R/T) non-equilibrium trajectories characterizing bacterial motion in free solution were rectified by the funnels. Such rectification can potentially be affected by many factors, e.g. the funnels geometry, the bacteria concentration and cell-cell interactions, the effective R/T mean free path, the physical properties of the bacteria, etc, most of which have yet to be thoroughly investigated. Nevertheless, it is clear that this rectification process can be exploited for practical applications. For instance, while a two-chamber system might be useful to concentrate cells, a multi-chamber device might even be used to separate cells possessing different swimming patterns or physical properties [3]. In other words, the net motion due to the ratchet process can be used to design separation systems for various purposes. In this paper, we propose a new approach to characterize and model such systems using a theoretical framework inspired by the separation sciences and developed to describe one dimensional biased random walks [4].

2 Theory

Let us consider a dilute suspension of self-propelled bacteria of size R_c such as *E. coli* moving in a R/T fashion with running events of mean duration τ_r at a mean velocity v_r interleaved by tumbling sessions of mean duration τ_t at a mean velocity v_t (v_r and v_t are parallel to each other). After each complete R/T cycle, the cell reorients and starts a new R/T cycle. The basic system is shown in Fig. 1. The cells move between parallel columns of funnels separated by a distance S; we use a two-dimensional system with periodic boundary conditions in the vertical direction for simplicity. Each funnel is made of two linear walls of length L_f that define an angle ϕ and a gap size L_g.

The R/T mean free path (MFP) $\lambda = v_r\tau_r + v_t\tau_t$ is the key to rectification since equilibrium thermodynamics (i.e., the limit where λ becomes negligible compared to all other length scales) does not allow diffusion to be rectified by funnels [1]. The regime of interest here is characterized by the inequality $R_c < L_g < L_f < \lambda < S$ or, in words: the cells must be able to pass through the gaps; the gaps must represent a small fraction of the overall wall area; the MFP of the cells must exceed the funnel size so that the latter can rectify the flow of cells in the vicinity of the wall; and finally the chamber size must be larger than the MFP otherwise the physics would be entirely controlled by the MFP and the direction of each individual trajectory.

Under the conditions described in the previous paragraph, the cells random R/T motion is rectified by the funnels (as observed experimentally and via previous computer simulations [1–3,5–7]). Let us first consider a closed system of N chambers separated by $N-1$ columns of funnels and terminated by two hard walls (Fig. 2(a) shows an example with $N = 5$ chambers and 4 walls). We start with a homogeneous initial state where the cell concentration is $\bar{\rho}$ in each chamber of width S. In the steady-state, the rectification ratio $\Theta \geq 1$ for two adjacent chambers is defined as

$$\Theta = \frac{\rho_{i+1}}{\rho_i}, \tag{1}$$

where ρ_i is the steady-state concentration in the i-th chamber. A simple recursion leads to the expression for the concentration in the i-th chamber with respect to the 0-th chamber:

$$\rho_i = \rho_0\ \Theta^i = \rho_0\ e^{i/\alpha}. \tag{2}$$

The sedimentation parameter

$$\alpha = (ln(\Theta))^{-1} \tag{3}$$

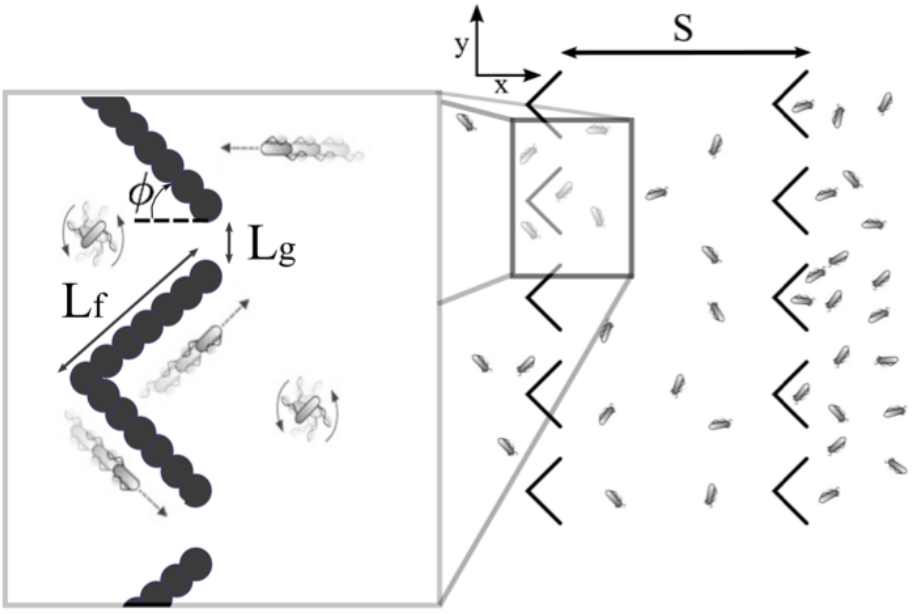

Figure 1: The geometry of the system. The chambers are separated by a distance S while the funnels are characterized by their gap L_g, length L_f and angle ϕ. The cells run and tumble process is shown in a schematic way.

is the decay length (in units of chambers) of the exponential distribution of cells in the steady-state. Using Eq. (2) and the fact that the total number of cells is conserved, we can write that

$$N\bar{\rho} = \sum_{i=0}^{N-1} \rho_i = \rho_0 \sum_{i=0}^{N-1} \Theta^i. \tag{4}$$

Solving the summation, we obtain:

$$\frac{\rho_i}{\bar{\rho}} = N\Theta^i \ \times \ \frac{\Theta - 1}{\Theta^N - 1}. \tag{5}$$

In practice, a large value of the rectification ratio Θ is the goal, so that α can be rather small: most of the cells will then accumulate in the last chamber ($i = N - 1$).

The fundamental question here is the relation between the rectification ratio Θ and the cell and device characteristics. The parameter space one has to explore is obviously quite vast. We propose to recast the problem using concepts borrowed from the separation sciences and the theory of biased random walks to help clarify the situation.

In the limit where the number of chambers is very large ($N \gg 1$), we can use a continuum limit approximation in one dimension to describe the stationary state of a close system. In this framework, an effective sedimentation force F_s pulls the bacteria while they diffuse with an effective diffusion coefficient D_s under an effective thermal energy $k_B T_s$, where the subscript s stands for sedimentation. We can thus define an effective sedimentation friction coefficient $\xi_s = k_B T_s / D_s$. In an open system, these cells would instead migrate from chamber to chamber at a net drift velocity $v_s = F_s/\xi_s$. We note that we can combine these definitions into the following simple relation:

$$\frac{F_s S}{k_B T_s} = \frac{v_s S}{D_s}. \tag{6}$$

The right-hand side of this equation is actually the Peclet number [8] for this one-dimensional drift-diffusion process:

$$Pe = \frac{v_s S}{D_s}. \tag{7}$$

Now, let us go back to the closed system. If we treat this as a sedimentation problem, then the concentration in the i-th chamber can be calculated as follows:

$$\rho_i \sim exp\left(\frac{F_s(iS)}{k_B T_s}\right) = exp\left(\frac{v_s S}{D_s} \cdot i\right) = exp(Pe \cdot i). \tag{8}$$

Therefore, the decay length is the inverse of the Peclet number, $\alpha = 1/Pe$. Hence, minimizing the decay length α (in order to concentrate the cells) of a closed system is equivalent to maximizing the separation power (as described by Pe) of an open system, that is maximizing the drift velocity of the swimmers while minimizing their diffusion. Using computer simulations, we will demonstrate that the above equivalence holds in the case of a dilute suspension of sphere-like R/T swimmers. We note that the end result depends on only three variables: the chamber size S (which is fixed for a given device), the drift velocity v_s (which is zero in absence of funnels) and the diffusion coefficient D_s (or, equivalently, on the effective sedimentation force F_s and the effective temperature $k_B T_s$). Consequently, in spite of the large number of parameters that can be tuned to optimize this system, these parameters can be combined into only three fundamental variables.

We can go a step further if the chamber size S is much larger than the MFP λ of the swimmers. In such a case, the jumps between chambers represent a Markov chain (the transitions are independent from each other). The dynamics of this overdamped drift-and-diffusion system is then controlled by the probabilities $p_\pm$ that a given cell will be crossing the barrier in the $\pm$

direction for its next move. In other words, this is a biased random walk on a lattice with a step size S.

Let us now map the system onto a simple one-dimensional lattice biased random walk (1DLBRW) model. Within the 1DLBRW framework, we can describe the dynamics using three variables (we use s subscripts to make the connection with the sedimentation equations above): (1) the lattice step size S; (2) the dimensionless bias [4]

$$\epsilon = \frac{F_s S}{2k_B T_s}; \tag{9}$$

and (3) the zero-bias mean diffusion time

$$\tau_B = \frac{S^2}{2D_s}. \tag{10}$$

The mean time to complete a jump in either direction in the presence of a bias ϵ is given by [4]:

$$\frac{\tau(\epsilon)}{\tau_B} = \frac{tanh(\epsilon)}{\epsilon} \approx 1 - \frac{1}{3}\epsilon^2 + O(\epsilon^4). \tag{11}$$

To first order in ϵ, the mean jumping time is thus constant. The probability $p_\pm$ for next jump to be to the adjacent site in the $\pm$ direction is [4]:

$$p_\pm(\epsilon) = \frac{1}{1 + e^{\mp 2\epsilon}} \approx \frac{1 \pm \epsilon}{2} + O(\epsilon^3). \tag{12}$$

The drift velocity v_s of the random walker is thus given by [4]

$$v_s = (p_+(\epsilon) - p_-(\epsilon)) \ \frac{S}{\tau(\epsilon)} = \frac{\epsilon S}{\tau_B} = \frac{F_s}{\xi_s}, \tag{13}$$

where ϵ can take any value. The result is as expected, the mean ratchet drift velocity being the ratio of the effective external force to the effective friction coefficient.

In absence of obstacles or potential barriers, the diffusion coefficient of a free particle, $D_s = S^2/2\tau_B$, should be independent of the bias. As we will see later, the situation is slightly different here since the funnel-shaped obstacles themselves are the source of the bias; we will neglect this connection in this paper but will discuss its impact in the Conclusion. However, as we described in a previous paper, this version of the 1DLBRW model leads to a diffusion coefficient that decreases with the bias ϵ at high bias because it fails to take into account the fluctuations in the jumping time [4]; the decrease if of second order in ϵ:

$$D_s = \frac{S^2}{2\tau_B} \approx 1 - \frac{2}{3}\epsilon^2 + \frac{14}{45}\epsilon^4 + O(\epsilon^6). \tag{14}$$

We will get back to this issue later.

Combining the previous equations, we obtain the following connection between the various descriptions of the problem:

$$2\epsilon = Pe = ln(\Theta) = \alpha^{-1} = \frac{v_s S}{D_s}. \tag{15}$$

We will be using these expressions below to analyze our simulation data. It is very important to note that the ratchet effective velocity v_s and diffusion coefficient D_s are not those of the cells in a funnel-free environment; these parameters are in fact direct measures of the ratchet (or funnels) performance for the given cell.

3 Methods

It is important to mention that our main interest is in the general process of active matter movement rectification in systems of funnels; in other words, E. coli is only used as an example. We neglect the impact of the rod-shape body of E. coli and we assume that it is a spherical particle for simplicity. As mentioned previously, we also neglect Brownian motion and we use the R/T distribution functions proposed by Sosa-Hernanadez et al [9]. Within the framework of deterministic dynamics, the equation of motion for the position $\vec{r}(t)$ of a cell of mass m is [10]

$$m\ddot{\vec{r}}(t) = \vec{F}_w - \xi\dot{\vec{r}}(t) + \vec{F}_{cell}(t), \tag{16}$$

where $\vec{F}_w$ is the force between the cell and the walls (we work in the dilute limit and thus neglect cell-cell interactions in this paper), $\vec{F}_{cell}$ is the cell driving force, and $-\xi\dot{\vec{r}}(t)$ is the drag force. The R/T driving forces $\vec{F}_{cell}(t)$ are selected in order for the resulting velocities $\vec{F}_{cell}/\xi$ to satisfy the distribution functions mentioned before.

The funnel walls in our system are simply modelled using series of fixed beads which interact with the bacteria via the WCA potential

$$\frac{U(r)}{4\epsilon_W} = \begin{cases} \left(\frac{\sigma}{r}\right)^{12} - \left(\frac{\sigma}{r}\right)^{6} + \frac{1}{4} & r < r_{\text{cut}} \\ 0 & r \geq r_{\text{cut}}, \end{cases} \tag{17}$$

where r is the distance between the wall and the centre-of-mass (CM) of the cell, ϵ_W measures the magnitude of the repulsive potential, and σ is the WCA length-scale describing the range of the potential. The WCA potential is truncated at a distance $r_{\rm cut} = 2^{1/6}\sigma$ from the CM, which is the position of the minimum for the standard Lennard-Jones potential. The funnel beads are fixed in space and are separated by a distance of 0.7σ from each other.

In the rest of this paper, we will not mention the units of measurements of the different physical parameters in order to be more concise. Distances will be given in units of σ, times in units of the fundamental time $\tau_m = m/\xi$, and forces in units of $\xi\sigma/\tau_m$. All simulations were performed using the ESpResso package [11].

We can use the papers by Galajda et al [1] al and Sosa-Hernanadez et al [9] to determine what our dimensionless simulation parameters correspond to in terms of experimental conditions. The length of an E. coli cell is ~ 3 μm, while our simulation sphere has diameter of ~ 2 σ; we can thus consider the unit of length to be $\sigma \sim 1.5$ μm. The funnels used by Galajda et al [1] were of size 27 μm, while our simulation funnels have a length of 7 σ (we also studied longer funnels of size 10-20 σ; results not shown). During one R/T cycle, an E. coli cell travels at a velocity ~ 35 μm/s along its direction of motion. In a typical simulation, the cell travels over one mean free path (~ 20 σ) at a velocity ~ 0.15 σ/τ_m in a period of time ~ 150 τ_m; the time unit in our simulation is thus $\tau_m \sim$ 0.01 second.

4 Results

As discussed before, several factors may impact the rectification effect of this geometric ratchet including the chamber size S, the funnel length L_f, the cell mean free path λ, the gap size L_g and the details of R/T model used. Given the large number of parameters, we have chosen to focus our attention on the key parameters λ and L_g; therefore, the funnel size $L_f = 7$ and opening angle $\phi = 45^\circ$, as well as the chamber width $S = 120$, are kept fixed. A given value of the R/T mean free path $\lambda = v_r\tau_r$ can be obtained using various combinations of the mean run velocity v_r and mean run duration τ_r; we thus use the notation $\{\lambda/v_r/\tau_r\}$ to describe the properties of the R/T process for a cell.

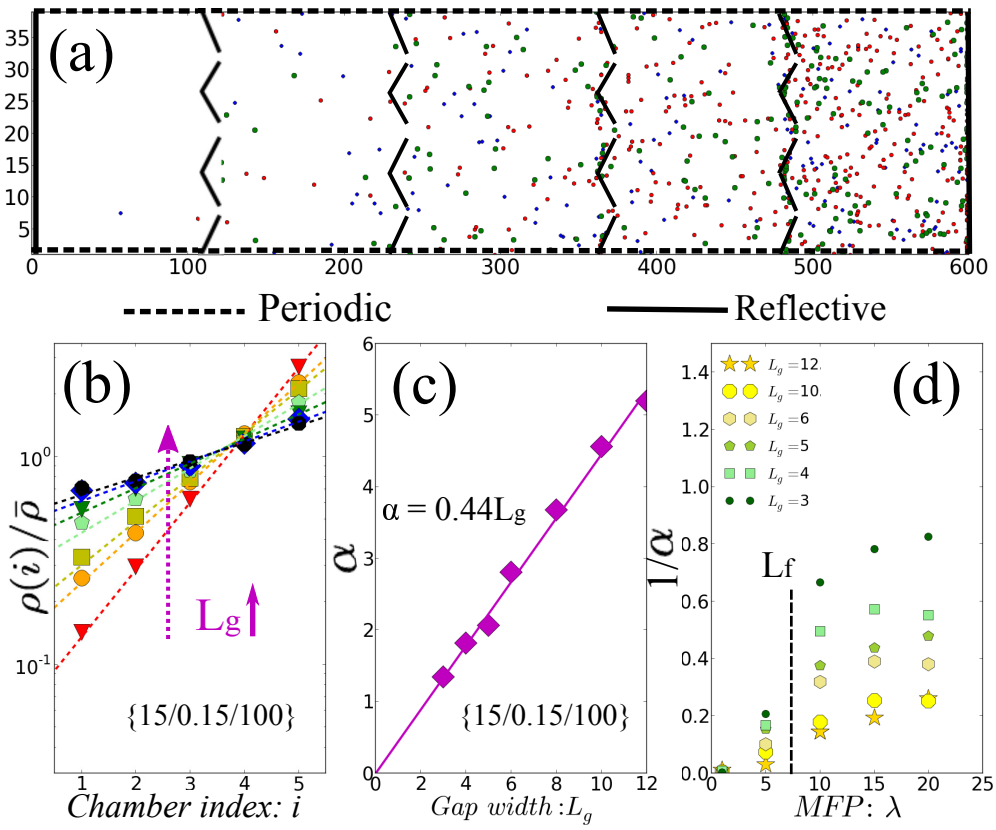

Figure 2: A closed system with 5 chambers and 4 funnel walls with a gap of size $L_g = 3$. The total length of the system is $L_x = 5S = 600$, and we used $L_y = 39$ with periodic conditions in the vertical direction. A total of 500 cells were evenly distributed between the 5 chambers at the beginning of the simulation. (a) A stationary state showing that cells have accumulated in the last chamber on the right. The mean free path of the cells is $\lambda = 15$ with the R/T parameters being $\{15/0.1/150\}$. (b) Semilog plot of the steady-state reduced density $\rho(i)/\bar{\rho}$ vs the chamber index i for gap widths L_g =3, 4, 5, 6, 8, 10, and 12. (c) The decay length α vs the width of the gap L_g; the values of α come from the fits in (b). The linear fit shows that $\alpha = 0.44(2) \times L_g$. (d) The inverse of the decay length, $1/\alpha$, vs the MFP λ for various gap widths L_g (the cell mean run velocity was kept fixed at $v_r = 0.1$; the different values of $\lambda = v_r\tau_r$ were thus obtained by varying the mean run time τ_r). We note the very rapid decay when λ becomes smaller than the funnel length L_f.

Let us first study a closed system. Figure 2(a) illustrates the stationary state of a population of cells within a system made of 5 chambers and 4 funnel walls (here we show 3 funnels pointing to

the right, and periodic boundary conditions are applied in the vertical direction). The $\bar{\rho} = 100$ cells are evenly distributed in every chamber at the beginning of the simulation. Figure 2(b) shows the reduced cell density $\rho(i)/\bar{\rho}$ as a function of the chamber number i on a semi-log plot. The straight lines indicate that we do indeed have an exponential decay of the cell population. The decay length α is the inverse of the slope of the linear fits; as Fig. 2(c) shows, α increases linearly with the gap size L_g, a remarkably simple scaling law. Smaller gap sizes increase the rectification effect, which is to be expected since in the limit where $L_g \gg L_f$, the walls are too porous to have any effect. Figure 2(d) shows that the MFP λ has a relatively small effect on the decay length, except when the MFP becomes very short ($\lambda < L_f$) since the funnel system cannot rectify Brownian motion, in agreement with previous findings [1, 2].

We now examine a system with periodic boundary conditions (PBC) along the net direction of motion, i.e., we remove the boundaries at two ends of the system showed in Fig. 2(a). In fact, one can build such a system using a racetrack format in two dimensions. In an open system like this, the cells have a well-defined mean drift velocity v_s and a diffusivity D_s along the direction of net motion, much like a particle pulled by a force F_s (e.g., gravity) through a viscous fluid. As discussed in the Theory section, this net motion can also be described by a 1DLBRW; in this case, the key parameters to follow during the simulations are the mean time to move from one chamber to the next and the directional probabilities $p_{\pm}$. Figure 3 shows how these four measures of the dynamics of the cells in an open system change when we vary the funnel gap L_g. Note that the different MFPs are color-coded. We also added cases with similar MFPs but different combinations of v_r and τ_r.

Figures 3(a)-(b) show that the MFP has a strong effect on both the drift velocity v_s and the diffusivity D_s. Moreover, even the velocity v_r chosen to achieve a certain MFP $\lambda = v_r\tau_r$ matters. However, the gap size L_g has a minor effect on D_s (a smaller gap size increases the density of obstacles in the system and hence reduces D_s; we will neglect this secondary effect in the following). The net velocity v_s collapses when the gap becomes too large, once again because the wall then becomes too porous. These results suggest that if we want to optimize rectification by changing the geometry, reducing the gap width is the obvious option.

The MFP λ is the linear distance traveled by the cell during a single R/T step. For a given

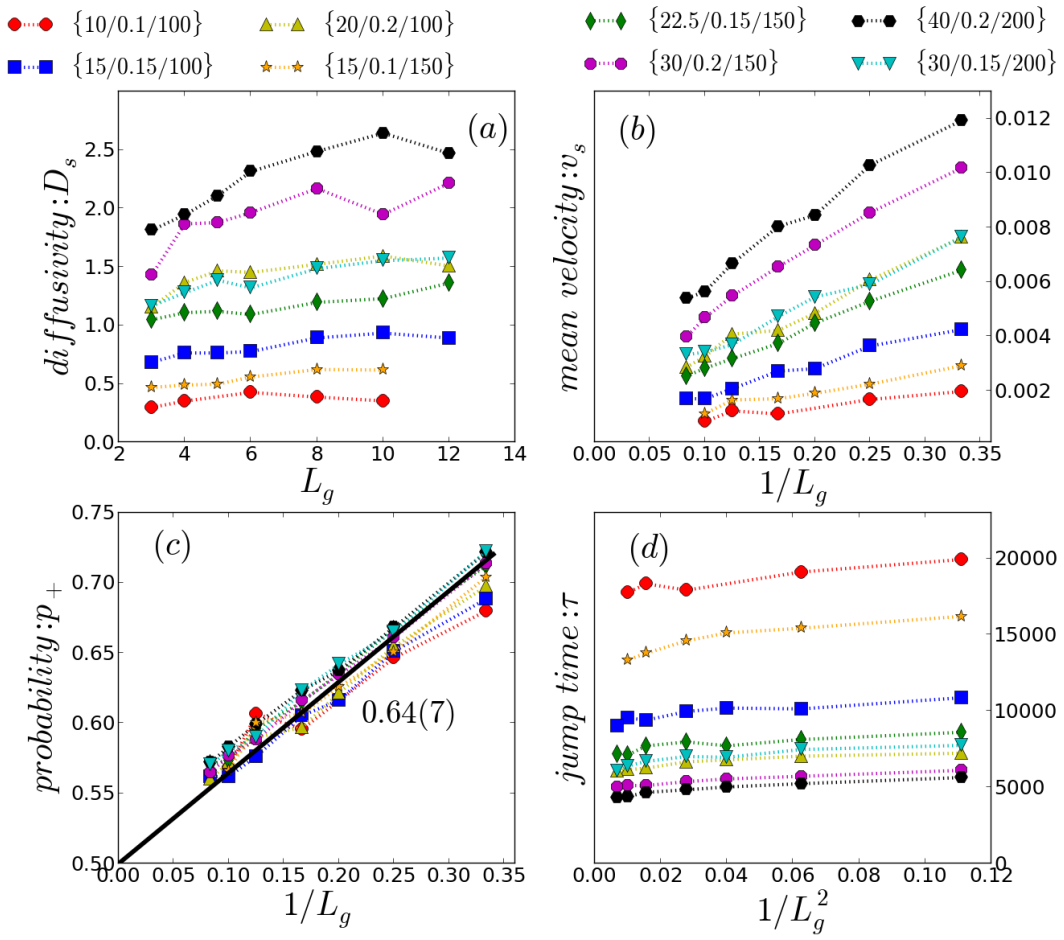

Figure 3: Four different parameters characterizing the net rectified motion of cells as a function of the width of the gap L_g for an open system. The different data sets marked as $\{\lambda/v_r/\tau_r\}$ correspond to different MFPs λ and combinations of v_r and τ_r. (a) The diffusivity D_s. (b) The mean cell velocity v_s. (c) The jumping probability p_+; linear fit corresponds $p_+ \approx \frac{1}{2} \times \left(1 + \frac{1.3(1)}{L_g}\right)$. (d) The average time to complete one jump.

run velocity v_r, a higher value of λ results in larger values of D_s and v_s, which is not a surprise. However, for two cells with the same MFP λ but different values of v_r, their diffusivities and mean velocities can be very different (note that the diffusivity $D_o \approx v_r^2 \tau_r \approx \lambda v_r$ would be different even in absence of funnels). For instance, if we take the cells with R/T parameters {30/0.15/200} and {30/0.2/150} in Figs. 3(a)-(b), the later has a diffusivity that is almost 1.5 times higher and a velocity that is 1.25 times higher. The difference on the net velocity v_s is partly caused by the

funnels: during their R/T motion, the cells are sometimes trapped in the dead-ends of the ratchet geometry while moving against the funnels preferred direction. For a given MFP λ, the cells with the smallest run times τ_r (or, equivalently, with the largest velocities v_r) will reorient faster and hence will lose less time in these dead-ends. This "dead-end effect" plays an important role in ratchet processes. These results obviously imply that we can separate cells on the basis of their swimming properties even when they possess identical MFPs. The difference in the net diffusion coefficient D_s is due to a combination of the "dead-end effect" and the fact that the value of D_o is different to start with.

Interestingly, the probability p_+ for the cell to move to the forward chamber is essentially the same for all MFPs: to a good approximation, the data collapse on the straight line $p_+ \approx \frac{1}{2} \times \left(1 + \frac{1.3(1)}{L_g}\right)$ over the range of gap sizes studied here (obviously, the range is limited to $L_g \geq 2R_c$). As the gap size increases, the jumping probability converges to 50%, as expected for an unbiased random walk. Although, the average jumping time τ stays rather flat when the gap size changes (the small variation is largely due to the change in the density of obstacles, as discussed above), the actual value strongly depends on the combination of v_r and τ_r used to obtain a give MFP λ. In other words, while the bias p_+ depends on the gap size but not on the value of v_r (or τ_r), we have the exact opposite for the average jumping time τ. These results show that the inverse gap size $1/L_g$ is equivalent, at least to first order, to an external force in a typical 1DLBRW model. We conclude that the fact that the velocity v_s depends on the MFP comes entirely from the jumping time τ.

The next step in our investigation is to compare the results obtained for close and open systems. Since we obtain the values of diffusivity and the net velocity from our open system simulations, we can calculate Pe and compare it to the decay length α obtained for the close system. Figure 4 shows that the data is consistent with the prediction (dashed line) that $1/\alpha = Pe = v_s S/D_s$ for a wide range of parameters. Therefore, the physics of this system, whether it is open or close, is similar to that of a particle pulled through a viscous liquid by an external force F_s. The question is thus which parameters control the value of effective force F_s, the effective friction coefficient ξ_s and effective temperature $k_B T_s$. To examine this issue further, we will map the problem onto a 1DLBRW, as described in the Theory section.

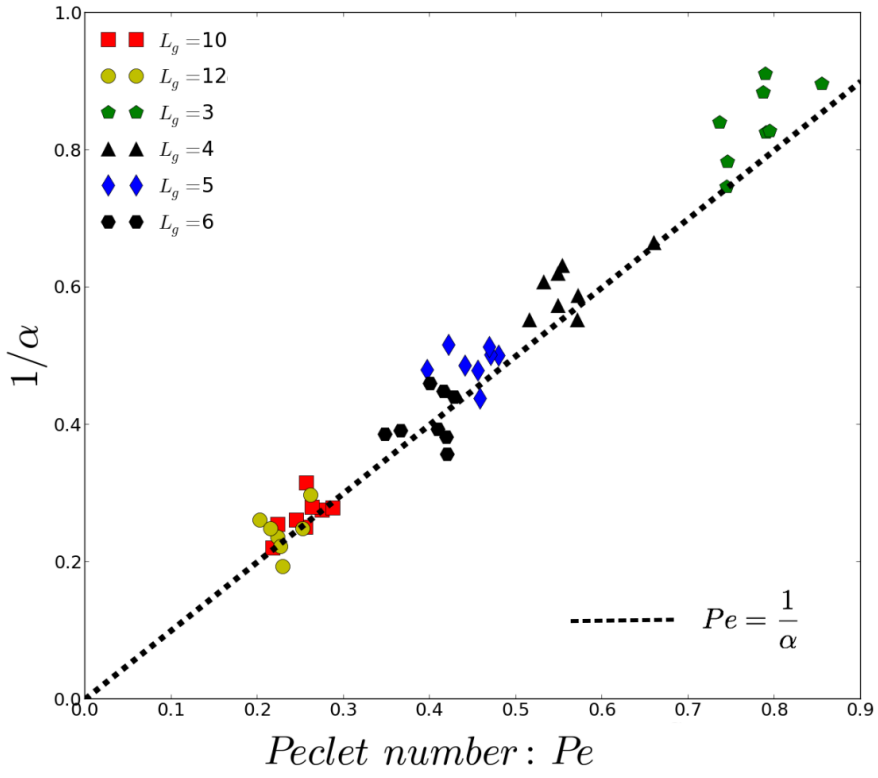

Figure 4: Comparing the Peclet number $Pe = v_s S/D_s$ and the inverse decay length $1/\alpha$. The theoretical prediction is given by the dashed line.

One can use different approaches to test the validity of the 1DLBRW mapping. Here we chose to start from the 1DLBRW equations to find the value of the relevant parameters (ϵ and τ_B) and then see if we can recover the simulation data. The bias ϵ can be computed from the value of p_+ using Eq. (12). Then Eq. (11) can be used to compute the value τ_B from the simulation value of the average duration τ and the numerical estimate of ϵ. Not surprisingly, Fig. 5(a) shows that $\epsilon \propto 1/L_g$, and that there is a rather weak dependence on λ and v_r. This is identical to what we observed for p_+ and confirms that $1/L_g$ is indeed the driving force. Figure 5(b) shows that the Brownian time is almost independent of the gap size L_g; in the limit where $L_g \to \infty$, it seems to converge towards the value $\frac{S^2}{4D_o}$, where $D_o = v_r^2 \tau_r/4$ is the diffusivity of the swimming cell in the free solution. Again, R/T process affects the characteristic diffusion times, but not the bias.

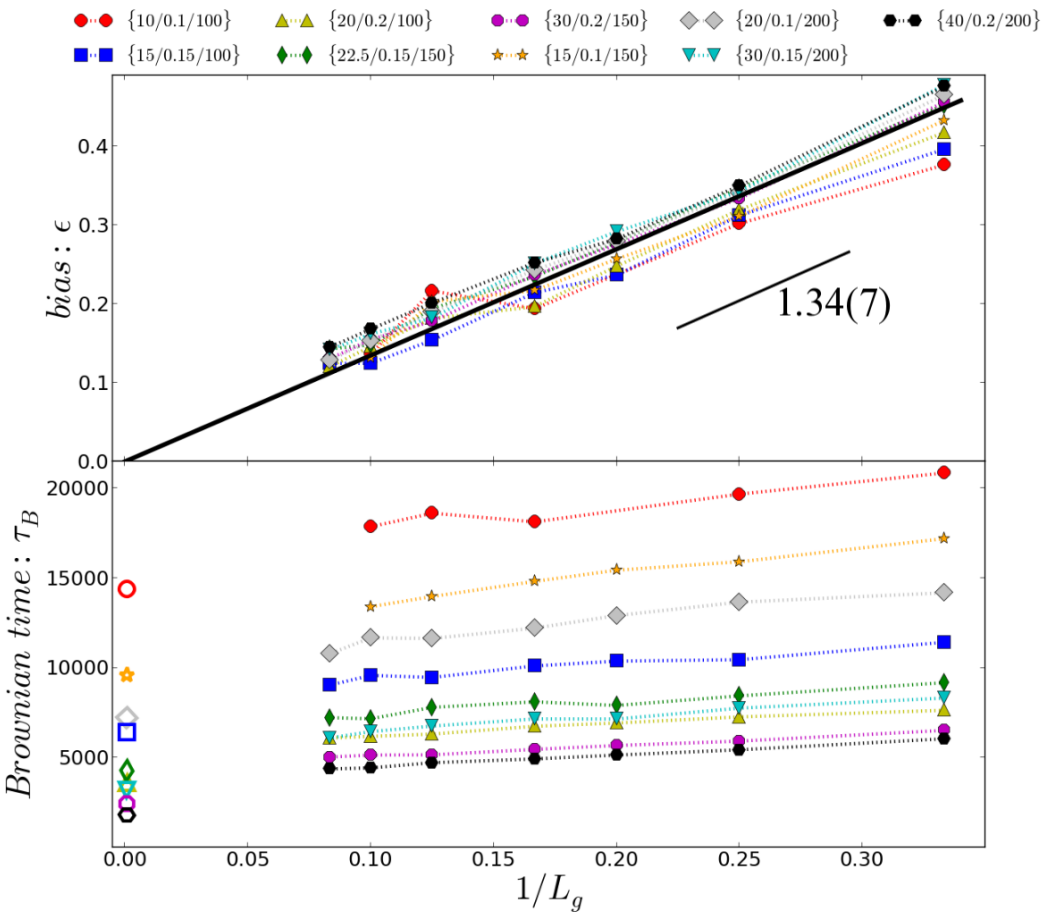

Figure 5: Calculated (a) bias ϵ and (b) Brownian time τ_B as a function of inversed gap size $1/L_g$. The unfilled markers on the left of panel (b) give the Brownian time of the cells in free solution.

Using the numerical results for ϵ and τ_B, we can predict the 1DLBRW theoretical net velocity v_s and diffusivity D_s using Eq. (13) and the fact that $D_s = S^2/2\tau_B$. Figure 6 shows that the data converge towards the theoretical values (the solid lines) when the MFP is small compared to the size of the system. The discrepancy is particularly large for D_s when the MFP is large. This suggests that the mapping approach is better for small MFPs.

Finally, we can also test whether the 1DLBRW bias parameter obtained from Eq. (12) and the values of $p_{\pm}(\epsilon)$ extracted from the simulations, is equal to the Peclet number $Pe = v_s S/D_s$ obtained directly from the simulation results for v_s and D_s, see Fig. 7. According to Eq. (15), we

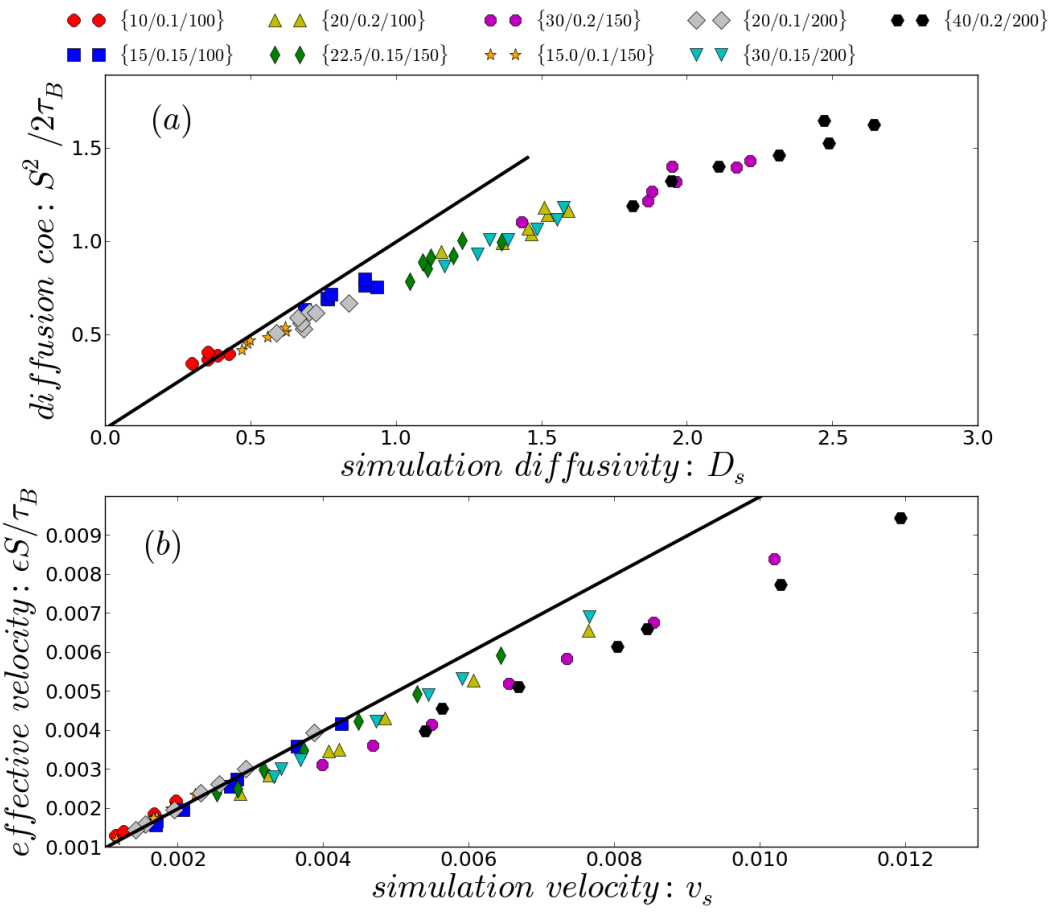

Figure 6: Comparisons between the diffusivities and velocities obtained directly from the simulations (x-axis) and those computed using the parameters of the one-dimensional lattice biased random walk model (y-axis). The straight lines show the predicted equality.

expect the slope to be 0.5 (dashed line); our result seem to agree with a slightly different slope of 0.57 instead.

5 Conclusion

We investigated the rectification of autonomous swimming cells in confined funnel systems using a simple two-dimensional ballistic run and tumble (R/T) model. We showed that the ratchet process

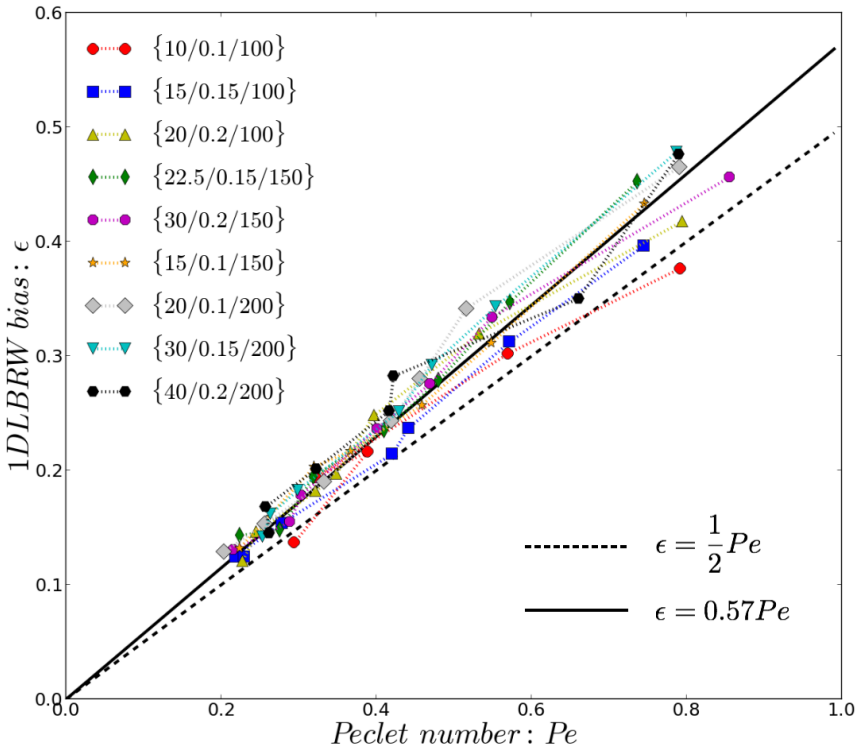

Figure 7: Calculated bias ϵ vs the Peclet number $Pe = \frac{v_s S}{D_s}$. The solid line is a linear fit; the dashed line represents the theoretical prediction.

is similar to the problem of a particle pulled in a liquid by an external force. This effective force is the result of the non-equilibrium R/T process combined with the asymmetry of the funnels. In other words, the rectification of the cell R/T motion can be seen as a simple transport problem, similar to those studied and exploited in separation science. For instance, in a closed system, the process resembles sedimentation. We also argued that the most natural way to simplify the problem is to transform it into a one-dimensional lattice biased random-walk since such a model has only 3 parameters, one being the size S of the chambers. This analogy demonstrates that the complexity of the original problem can be reduced to only two fundamental parameters, the random walk bias and jump time.

Researchers in separation science have developed many empirical and theoretical methods to

optimize the separation of particles that have different velocities v_s and diffusion coefficients D_s. As always, it is crucial to reduce D_s in order to concentrate and/or separate objects that drift in a liquid. We have shown that the key to concentrating cells using the ratchet process is increasing the system's effective Peclet number Pe. However, it should also be possible to build a cyclic system (a racetrack) which would allow different types of cells to form separate populations, hence allowing the user to isolate them. It might also be possible to build more complicated two-dimensional maze-like structures. In all of these cases, the design and optimization processes will be greatly facilitated by mapping the system onto a lattice biased random-walk model since this mapping reduces the number of meaningful variables to only three; moreover, lattice models allow one to find exact solutions.

For the multi-chamber concentrating device (see refs. [1,2] and Fig. 2(a)), optimization means decreasing the decay length α or, equivalently, increasing the Peclet number $Pe = v_s S/D_s = 1/\alpha$. In terms of the transport variables introduced in this paper, this means increasing the bias ϵ (or the net velocity v_s) while increasing the effective Brownian time τ_B (or decreasing the diffusion coefficient D_s). One of our main findings is the remarkably simple scaling law $v_s \propto \epsilon \propto 1/\alpha \propto 1/L_g$. This can be used to guide the optimization of this device for specific purposes; it can also be used to tune the properties of an eventual racetrack device.

However, our work suffers from some weaknesses and further studies will be needed to improve it. These include the following:

- Many bacteria (e.g. E. Coli) have cigar-like shapes, and this obviously leads to different cell-cell and cell-wall interactions; our model can easily be extended to study such cells since a rigid rod of beads would have the proper dynamical behaviour.
- We noticed that the jumping times are slightly different between the two directions of the ratchet (p_+ jumps being slightly shorter than p_- jumps). This is not the case in a standard 1DLBRW model. This small effect may explain some of the discrepancies we observed for long MFPs. In a standard biased random walk, the external field is uniform in space. This is not the case here since the effect of the funnels can only be felt by cells that are within one MFP (or so) from a funnel. A generalized biased random walk model may need to be derived to take this into account.

- The 1DLBRW fundamental time τ_B is normally the time taken for the random walker to diffuse over the distance S, the lattice spacing, in absence of the external field. In our ratchet model, however, there is a (weak) coupling between the effective external field $\epsilon \propto 1/L_g$ and the value of τ_B since increasing the field by reducing the gap size L_g slightly increases the diffusion time τ_B. This may need to be included in a more complete version of the model.

- Finally, we have neglected the impact of R/T fluctuations (the run trajectories fluctuate laterally). Again, it would be relatively easy to add this to the simulation model.

It would be easy to modify the rules under which a cell determines a new direction of motion in order to generate flocking and other types of collective behaviors. Of particular interest would be the behaviour of one or more species of flocking cells in a racetrack format. The approach presented here can easily be extended to study such problems.

References

[1] Galajda, P., Keymer, P., Chaikin, P., Austin, R., *Journal of Bacteriology* , 2007, *189*, 8704-8707.

[2] Galajda, P., Keymer, P., Dalland, J., Park, S., Kou, S., Austin, R., *Journal of Modern Optics* , 2008, *55*, 3413.

[3] Elizabeth Hulme, S., DiLuzio, W., Shevkoplyas, S., Turner, L., Mayer, M., Berg, H., Whitesides, G., *Lab Chip*, 2008, *8*, 1888.

[4] Gauthier, M., Slater, G., *phys Rev Lett E*, 2004, *70*, 015103.

[5] Lambert, G., Liao, D., Austin, R., H., *Phys Rev Lett*. 2010 , *104*, 168102.

[6] Wan, W., Reichhardt, C., O., Nussionv, Z., Reichhardt, O., *Phys Rev Lett* 2008, *101*, 018102.

[7] Berdakin, I., Jeyaram, Y., Moshchalkov, V. V., Venken, L., Direckx, S., Vanderleyden, S. J., Sihanek, A. V., Condat, C. A., Marconi, V. I., *Phys Rev E* 2013, *87*, 052702.

[8] Patankar, S. V., *Numerical Heat Transfer and Fluid Flow*, New York: McGraw-Hill. 1980.

[9] Sosa-Hernanadez, J., E., Santillan, M., Santana-Solano, J., *phys Rev Lett E*, 2017, *95*, 032404.

[10] Coffey, W., Kalmykov, Y. P., Waldron, J. T., *The Langevin Equation*, World Scientific, River Edge 1996.

[11] Limbach, H. J., Arnold, A., Mann, B. A., Holm, C., *Comput. Phys. Commun.* 2006, *174*, 704-727.

Chapter 5

Conclusion

Ratchet effects dominate a major part in my Master projects. These ratchets require non-equilibrium conditions and symmetry breaking structures. In my first project, I took advantage of the ratchet effect to propose new ways to manipulate charged particles by electrophoresis; in my second project, I mapped the rectification of swimming cells onto a simple one dimensional lattice biased random walk (1DLBRW) model [1].

When I started my Master, I focused my efforts on the separation of charged spherical particles which are inseparable in free solution electrophoresis. However, electrophoretic separation of these particles can be achieved in some microfluidic devices. In Chapter 2, I utilized Craighead's microfluidic device [2], in which the mobility of a spherical particle increases with the electrical field. For a given electric field, the mobility is also size-dependent. Thus it is possible to produce size-based ratchet effects in such systems in order to manipulate particles.

In my study, the most exciting finding is absolute negative mobility: two particles with the same type of charge can be driven in opposite directions. In addition, with proper design, the temporal asymmetric potential can even launch one specific particle at a time from a mixture. In Chapter 3, I showed that it is also possible to force a particle to stay at its original position while others move away. Considering the three possible applications mentioned above, one can realize the advantages of using such temporal asymmetric fields as a method of separating, purifying and concentrating charged particles.

To gain time-efficiency when using ratchet-like effects, the field intensity needs to be fairly strong in order to drive particles faster. In the weak field limit, I proposed to use an Ogston-like theory to explain the size-dependence of the particle mobility. This theory is essentially a well-designed interpolating function. I then used this function to propose a simple empirical stretched exponential function for the field-dependence of the mobility.

A few years ago, my previous colleagues Bertrand and Tao started investigating an approach to map the dynamics of active matter in a funnel structure onto a simple random walk model. I picked up the project after I realize the key of such a system is also a ratchet effect. Mapping such dynamics onto a new model can provide us a way to optimize similar devices.

Self-driven bacterias that are moving in a run and tumble (R/T) fashion can be rectified by introducing asymmetric barriers [3, 4]. For active cells with different velocities and run durations, yet the same mean free path λ, I predicted that it should be possible to separate them by using funnel arrays with periodic boundary conditions.

Then I showed that the steady-state decay length α of the multi-chamber rectification device is the inverse of the Peclet number of the cell transport process. Optimization requires increasing the mean velocity of the active cells, while reducing the related diffusion coefficient. This approach is always in the spirit of the separation science.

Rectification and separation can potentially be affected by many factors, and optimizing a device with many parameters is not an easy task. Mapping is one of the options to simplify the model and reduce the number of parameters. The fact that a large chamber (of size S) makes the system discrete, suggests that it is possible to map the process onto a 1DLBRW model. As it turns out, the mapping is excellent when $\lambda \ll S$.

As discussed above, I explored the theory of ratchet processes in two independent examples. My studies can potentially be useful for experimentalists, but there is certainly space for improvement. In the following sections, I explain how the "cross-talk" between simulations and reality came into play, and additionally what might be investigated in the future.

5.1 Ratchets in electrophoresis

I should not hide the fact that my simulation model is a simplified one. I have neglected the hydrodynamic interactions during the simulation. I have not considered the electrical forces acting on the entire particle. In reality, charged particles are not only affected by these two facts above, but may also have their own intrinsic complexity. For example, charged particles may be deformable, non-spherical and their surface charges might even be mobile, which would lead to polarization. Considering these facts in future simulation models might lead to some new, exciting and useful findings.

Two questions remain unclear for the microfluidic device I studied. The first relates to the crossover field: what parameters determine the value of this critical field? To the best of my knowledge this crossover regime has some correlation with the geometry of the microfluidic device. I found that the crossover field shifts once I changed the device, as can be seen in Chapter 2. The second question is about the maximum and minimum particle mobilities. Increasing the particles mobility in the weak field regime might be one of the most efficient methods for manipulating particles with a ratchet. In Chapter 2, I placed particles in a device with longer channels and this increased the mobility in the weak field regime. My naive prediction is that since charged particles have higher velocities in the channels, increasing the length of the channel is equivalent to increasing the mean velocity. The problem is how to optimize such effect by changing the geometry of the devices.

It would also be interesting to expand the work presented here to the case of rods. In particular, rods with the same number of charges yet with different charge distributions: can those charged rods be separated? The rotation of the rods in a non-uniform field will add a fundamental time scale (which is also controlled by the distribution of charges). This timescale can be exploited using pulsed fields as well.

5.2 Mapping active cells

It is important to mention that my simulations neglected the hydrodynamic interactions between the cells and the boundaries. Also I used a simple sphere

to simulate typical cigar-shaped swimming bacteria. When a rod-shaped active cell hits a boundary, it will naturally reorientate along the boundary. There was no such "reorientation" behaviour in my simulations of spherical cells. Making the simulation model better fit the real situation could be one future topic for investigation.

In the mapping process, I showed that the bias ϵ in the 1DLBRW model is inversly proportional to the gap size L_g. However, the relationship between L_g and the time parameter τ_B is still unclear. In addition, I have only investigated 2 parameters that influence the rectification process, i.e. the cell mean free path λ and the width of funnel gap L_g. The impacts of the funnel length, the funnel angle and the chamber size on the rectification efficiency are yet to be fully understood. Rectification of active cells in different funnels are nontrivial to test. These effects should be accounted for in future work on mapping processes.

Bibliography

[1] Gauthier, M., Slater, W. G., *Phys Rev Lett E*, 2004, *70*, 015103.

[2] Han. J., Craighead. H. G., *Science* 2000, *288(5468)*, 1026-1029.

[3] Galajda, P., Keymer, P., Chaikin, P., Austin, R., *Journal of Bacteriology* , 2007, *189*, 8704.

[4] Galajda, P., Keymer, P., Dalland, J., Park, S., Kou, S., Austin, R., *Journal of Modern Optics* , 2008, *55*, 3413.